



HAL
open science

High-frequency homogenisation in periodic media with imperfect interfaces

Raphaël C Assier, Marie Touboul, Bruno Lombard, Cédric Bellis

► **To cite this version:**

Raphaël C Assier, Marie Touboul, Bruno Lombard, Cédric Bellis. High-frequency homogenisation in periodic media with imperfect interfaces. Proceedings of the Royal Society of London. Series A, Mathematical and physical sciences, 2020, 476, pp.20200402. <hal-02615237v4>

HAL Id: hal-02615237

<https://hal.science/hal-02615237v4>

Submitted on 22 Oct 2020

HAL is a multi-disciplinary open access archive for the deposit and dissemination of scientific research documents, whether they are published or not. The documents may come from teaching and research institutions in France or abroad, or from public or private research centers.

L'archive ouverte pluridisciplinaire HAL, est destinée au dépôt et à la diffusion de documents scientifiques de niveau recherche, publiés ou non, émanant des établissements d'enseignement et de recherche français ou étrangers, des laboratoires publics ou privés.



HAL Authorization

High-frequency homogenisation in periodic media with imperfect interfaces

Raphaël C. Assier^{a,*}, Marie Touboul^b, Bruno Lombard^b, Cédric Bellis^b

^a*Department of Mathematics, The University of Manchester, Oxford Road, Manchester, M13 9PL, UK*

^b*Aix-Marseille Univ, CNRS, Centrale Marseille, LMA, Marseille, France*

Abstract

In this work, the concept of high-frequency homogenisation is extended to the case of one-dimensional periodic media with imperfect interfaces of the spring-mass type. In other words, when considering the propagation of elastic waves in such media, displacement and stress discontinuities are allowed across the borders of the periodic cell. As is customary in high-frequency homogenisation, the homogenisation is carried out about the periodic and antiperiodic solutions corresponding to the edges of the Brillouin zone. Asymptotic approximations are provided for both the higher branches of the dispersion diagram (second-order) and the resulting wave field (leading-order). The special case of two branches of the dispersion diagram intersecting with a non-zero slope at an edge of the Brillouin zone (occurrence of a so-called Dirac point) is also considered in detail, resulting in an approximation of the dispersion diagram (first-order) and the wave field (zeroth-order) near these points. Finally, a uniform approximation valid for both Dirac and non-Dirac points is provided. Numerical comparisons are made with the exact solutions obtained by the Bloch-Floquet approach for the particular examples of monolayered and bilayered materials. In these two cases, convergence measurements are carried out to validate the approach, and we show that the uniform approximation remains a very good approximation even far from the edges of the Brillouin zone.

Keywords: High-frequency homogenisation, periodic media, imperfect interfaces

1. Introduction

Classically, dynamic homogenisation is understood as a low-frequency approximation to wave propagation in heterogeneous media such as laminates, composites, or more generally any microstructured media. It consists in approximating such media by effective homogeneous media with specific properties. Homogenisation is the mathematical process that allows one to find such properties. Much work on this topic has been carried out since the 1970s and it is not the aim of this introduction to be exhaustive in that regard. A particularly successful approach is the two-scale asymptotic expansion method and the notion of *slow* or *fast* variables (see e.g. [1], [2], [3]). Periodic media, with which we are concerned in this paper, are dealt with very efficiently by such method.

*Corresponding author

Email address: raphael.assier@manchester.ac.uk (Raphaël C. Assier)

Preprint submitted to PRSA

October 22, 2020

In periodic media, waves can propagate at angular frequencies ω that are not necessarily small. The set of wavenumbers k (also known as Bloch wavenumbers) at which waves propagate depends on the angular frequency through dispersion relations. In particular it can be shown that these dispersion relations can be entirely understood using diagrams restricting the Bloch wavenumbers to lie within the Brillouin zone. In one dimension, when the periodicity of the structure is h say, such Brillouin zone is given by $k \in [0, \pi/h]$. Typically in such problems, the dispersion diagram displays band-gaps, i.e. regions in the angular frequency space where waves cannot propagate. There tends to be infinitely many branches of the dispersion diagram, i.e. for a given Bloch wavenumber, one can find an infinite (countable) set of angular frequencies leading to propagating waves. Again, a lot has been written about this, and we do not aim to give an exhaustive literature review on this point, though we can refer the interested reader to [4] for example. See also [5] for a discussion of the band gaps in periodic materials from a physics point of view.

The idea of *high-frequency homogenisation* is to approximate how the dispersion relation (and hence the media) will behave for angular frequencies ω that are close to the angular frequencies ω_0 corresponding to an edge of the Brillouin zone on the dispersion diagram. In [6], a work that has largely inspired the present paper, Craster et. al. applied a two-scale asymptotic expansion method in order to achieve this for perfect interfaces. Adopting the terminology of [7], we will refer to the homogenisation near the left edge of the Brillouin zone $k \approx 0$ as Finite Frequency Low Wavenumber (FFLW), while the homogenisation near the right edge ($k \approx \pi/h$) will be referred to as Finite Frequency Finite Wavenumber (FFFW). Upon introducing \tilde{k} as

$$\text{(FFLW)} : \tilde{k} = k \quad \text{and} \quad \text{(FFFW)} : \tilde{k} = \pi/h - k, \quad (1)$$

the end result of the high-frequency homogenisation technique is an approximation of the type

$$\omega^2 = \omega_0^2 + \mathcal{T}(\tilde{k}h)^2 + o\left(\frac{h^2\tilde{k}^2}{L^2}\right), \quad (2)$$

where L is a macroscopic characteristic length of the material and the parameter $\mathcal{T} \in \mathbb{R}$ can be determined explicitly. This angular frequency approximation comes together with an associated leading-order approximation to the wave field $U_h(X)$ of the form

$$U_h(X) = U_h^{(0)}(X) + \mathcal{O}\left(\frac{h\tilde{k}}{L}\right). \quad (3)$$

One should note that in [7], the authors generalised the technique to work in any dimension, and also pushed the asymptotic work one order further than [6]. It is also worth mentioning the more recent work [8], in which the technique was developed while including a source term in the initial evolution equation. As shown in [9], high-frequency homogenisation of wave equations in the time domain can also be carried out, and the methodology has also been applied in a discrete setting to structural mechanics [10] and elastic lattices [11].

In the present work, following the approach of [6], we wish to focus on extending this high-frequency homogenisation technique to one-dimensional periodic media that have an imperfect interface at the edges of the periodic cell, which, to our knowledge, has not been considered before.

Indeed, because of defects like air and cracks or thin layers of glue for example, the contacts between solids are often not perfect, and a jump of the elastic stress and of the elastic displacement can occur across the contact area (the interface). There are different approaches when it

comes to modelling such imperfect contact, and we refer to [12] for a comparison between different models. In particular, authors from various disciplines (e.g. non-destructive evaluation of materials or geophysics), have modelled such situations using the so-called *spring-mass* conditions that we will use in the present work. These conditions, satisfied by wave fields across an interface, are analogous to the mechanical laws of springs [13–16] or springs and masses [17, 18]. Stiffness and mass values are expected to be connected, although not necessarily in a trivial way, to the contact quality [19, 20]. More recently, rational derivations based on asymptotic expansion have been proposed, yielding similar spring-mass models of imperfect interface [21]. These imperfect conditions arise from a homogenisation process of a thin interphase. The results presented in the paper are hence relevant for wavelength comparable to the periodicity, but much larger than the thin interphase approximated by the imperfect contact laws. Here, we restrict ourselves to linear imperfect contact, though we kindly refer the reader to our work [22] on low-frequency homogenisation in the time-domain, where both linear and nonlinear imperfect contacts are considered. There exists a significant amount of work considering the homogenisation of such materials in the static regime (see for example [23], [24] and the more recent work [25]) but it seems that dynamic homogenisation has seldom been treated.

The rest of the paper is organised as follows. In §2.1 we formulate the one-dimensional physical problem at hand, namely that of linear elastic wave propagation through a layered material with periodic, possibly space dependent, material properties. The non-dimensionalisation of the problem is performed in §2.2, leading to the introduction of our small parameter δ , which is fully exploited via the two-scale asymptotic expansion method in §2.3. §3.1, §3.2 and §3.3 are respectively dedicated to the asymptotic expansion at order δ^0 , δ^1 and δ^2 , before combining these results in §3.4 to explicitly obtain the zeroth-order approximated wave-field and the associated formula for the parameter \mathcal{T} introduced in (2). Effectively, §3 provides approximations of both the dispersion diagram (second-order) and the wave-field (zeroth-order) at the edges of the band gaps. In the limiting case of a point on the edge of the Brillouin zone where two branches of the dispersion diagrams intersect with non-zero slope (such intersections are also known in the literature (see e.g. [26], [27] and [7]) as *Dirac points* or *Dirac cones*), the method developed in §3 needs to be adapted. This is what is done in §4, resulting in a linear approximation to the dispersion diagram. In order to provide a smooth transition between the asymptotics of §3 and §4, we consider the intermediate case of narrow band gaps in §5 and obtain a *uniform approximation* that remains valid in the Dirac point limit.

We then illustrate the method on two concrete examples, a homogeneous material (§6.1) and a bilayered material (§6.2) with periodically distributed imperfect interfaces. Such examples are also treated by the Bloch-Floquet analysis (see Appendix B), which allows us to illustrate and quantify the validity of our method. In particular, we discuss the occurrence of Dirac points, for which the approach of §4 should be taken. It is shown that the asymptotic expansion of §3 is a good local approximation near the edges of the band gaps, and that, even for not so narrow band gaps, the uniform approximation of §5 performs extremely well for almost the entirety of a given branch of the dispersion diagram. Perspectives and conclusions are given in §7.

2. Problem formulation

2.1. The physical problem

We consider linear elastic waves propagation at a given angular frequency ω through a periodic medium of periodicity $h > 0$ and with a macroscopic characteristic length $L > 0$. We

denote the physical space variable X ; the density $\rho_h(X)$ and the Young's modulus $E_h(X)$ of the elastic medium are assumed to be h -periodic piecewise smooth, L^∞ and strictly positive. We may assume without loss of generalities that the edges of the periodic cell are located at $X_n = nh$ for $n \in \mathbb{Z}$, as illustrated in Figure 1 (left). We further assume that the interfaces across the edges of the periodic cells are imperfect, and of the linear spring-mass type, characterised by some mass and stiffness parameters denoted respectively M and K that are both strictly positive. This results in the following governing equation and jump conditions for the displacement field $U_h(X)$:

$$\frac{d}{dX} \left(E_h(X) \frac{dU_h}{dX} \right) + \rho_h(X) \omega^2 U_h = 0, \text{ with } \begin{cases} \llbracket U_h \rrbracket_{X_n} = \frac{1}{K} \langle\langle E_h \frac{dU_h}{dX} \rangle\rangle_{X_n}, \\ \llbracket E_h \frac{dU_h}{dX} \rrbracket_{X_n} = -M\omega^2 \langle\langle U_h \rangle\rangle_{X_n}, \end{cases} \quad (4)$$

where $\llbracket \cdot \rrbracket_{X_n}$ and $\langle\langle \cdot \rangle\rangle_{X_n}$ are respectively called the jump and mean brackets at the interface X_n , and are defined for any function $g(X)$ by

$$\llbracket g \rrbracket_{X_n} = g(X_n^+) - g(X_n^-) \text{ and } \langle\langle g \rangle\rangle_{X_n} = \frac{1}{2}(g(X_n^+) + g(X_n^-)). \quad (5)$$

Due to the h -periodicity of ρ_h and E_h , it is possible to write them as $\rho_h(X) = \rho\left(\frac{X}{h}\right)$ and $E_h(X) = E\left(\frac{X}{h}\right)$ for some 1-periodic functions ρ and E .

Note 2.1. *Throughout this work, we assume that any discontinuity of ρ and E on $(0, 1)$ are of a perfect contact nature. This means that apart from at the interfaces $X = X_n$, we will assume that the displacement $U_h(X)$ and the stress $E_h(X) \frac{dU_h}{dX}$ are continuous.*

Classically, such wave propagation problem in periodic media can be understood by using the so-called Bloch-Floquet analysis that consists in seeking solutions of the form

$$U_h(X) = \mathfrak{U}_h(X) e^{ikX},$$

that propagate at the Bloch wavenumber k , and where $\mathfrak{U}_h(X)$ is h -periodic, that is, $\mathfrak{U}_h(X + h) = \mathfrak{U}_h(X)$. In certain simple cases (see e.g. §6.1 and §6.2), this leads to an explicit dispersion relation relating ω to k , the graphical representation of which is the so-called dispersion diagram.

One should note that for $k = 0$, we have $U_h(X) = U_h(X + h)$, i.e. the solution is periodic, while for $k = \frac{\pi}{h}$, we have $U_h(X) = -U_h(X + h)$, i.e. the solution is antiperiodic. Such values of k correspond to the edges of the so-called Brillouin zone. The aim of the present work is to approximate the Bloch-Floquet solutions propagating at wavenumbers that are close to $k = 0$ (FFLW) or $k = \frac{\pi}{h}$ (FFFW) with finite angular frequency $\omega = O(1)$.

2.2. Non-dimensionalisation

In order to simplify the mathematical notations, we start by non-dimensionalising the physical problem (4). In order to do so, we define the characteristic dimensional density $\rho^* = \langle \rho \rangle$, Young's modulus $E^* = \langle 1/E \rangle^{-1}$ and wavespeed $c^* = \sqrt{E^*/\rho^*}$, where the average operator $\langle \cdot \rangle$ is defined for any function g as

$$\langle g \rangle = \int_0^1 g(y) dy. \quad (6)$$

These can be used in order to define the following non-dimensional quantities

$$x = \frac{X}{L}, \quad \delta = \frac{h}{L}, \quad \mu = \frac{\omega h}{c^*}, \quad \kappa = Lk, \quad \alpha = \frac{\rho}{\rho^*}, \quad \beta = \frac{E}{E^*}, \quad \ell = \frac{Kh}{E^*}, \quad m = \frac{M}{h\rho^*}, \quad u_\delta(x) = \frac{U_h(X)}{L}. \quad (7)$$

The starred quantities ρ^* and E^* are chosen for convenience to be the effective properties of the medium obtained by low-frequency homogenisation, implying that $\langle \alpha \rangle = \langle 1/\beta \rangle = 1$, but this choice is somewhat arbitrary. Moreover, we can also show that

$$\rho_h(X) = \rho\left(\frac{X}{h}\right) = \rho\left(\frac{x}{\delta}\right) \quad \text{and} \quad E_h(X) = E\left(\frac{X}{h}\right) = E\left(\frac{x}{\delta}\right).$$

Using these quantities, (4) can be rewritten as the non-dimensional governing equation

$$\delta^2 \frac{d}{dx} \left(\beta \left(\frac{x}{\delta} \right) \frac{du_\delta}{dx} (x) \right) + \mu^2 \alpha \left(\frac{x}{\delta} \right) u_\delta(x) = 0, \quad (8)$$

subject to the jump conditions

$$\llbracket u_\delta \rrbracket_{x_n} = \frac{\delta}{\ell} \left\langle \left\langle \beta \left(\frac{x}{\delta} \right) \frac{du_\delta}{dx} \right\rangle \right\rangle_{x_n} \quad \text{and} \quad \delta \left\langle \left\langle \beta \left(\frac{x}{\delta} \right) \frac{du_\delta}{dx} \right\rangle \right\rangle_{x_n} = -m\mu^2 \langle u_\delta \rangle_{x_n}, \quad (9)$$

in the geometry setting of Figure 1 (centre). The equations (8)-(9) constitute our non-dimensional problem. Note that in this non-dimensional setting, the Bloch-Floquet analysis is still valid, and consists in looking for solutions of the form

$$u_\delta(x) = u_\delta(x) e^{i\kappa x}, \quad (10)$$

where κ is the non-dimensional Bloch wavenumber and u_δ is δ -periodic. Note that this implies that u_δ and its derivative u'_δ satisfy

$$u_\delta(x + \delta) = u_\delta(x) e^{i\kappa\delta} \quad \text{and} \quad u'_\delta(x + \delta) = u'_\delta(x) e^{i\kappa\delta}. \quad (11)$$

Remark 2.1. *The FFLW case corresponds to $\kappa\delta \approx 0$ and the FFFW case corresponds to $\kappa\delta \approx \pi$. When $\kappa\delta$ is exactly 0 (resp. π), then the solution $u_\delta(x)$ is δ -periodic (resp. δ -antiperiodic).*

2.3. Two-scale asymptotic expansion

We will now make the assumption that the macroscopic characteristic length L is much bigger than the periodicity h , implying that $\delta \ll 1$. The material parameters α and β will hence vary on a fine scale associated with the rescaled coordinate $y = x/\delta$ (see Figure 1 (right) for the associated geometrical configuration).

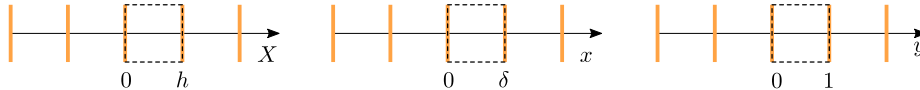


Figure 1: Geometry settings in the X , x and y variables, a periodic cell is highlighted with a dashed line.

Following the two-scale expansion technique, we further assume that the displacement field will have small scale features described by y , and slow continuous variations described by x . We hence pose the following ansatz for the wave field u_δ and the reduced frequency μ :

$$u_\delta(x) = \sum_{j \geq 0} \delta^j u_j(x, y) \quad \text{and} \quad \mu^2 = \sum_{\ell \geq 0} \delta^\ell \mu_\ell^2, \quad (12)$$

and treat x and y as two independent variables (scale separation), implying that $\frac{d}{dx} \leftrightarrow \frac{\partial}{\partial x} + \frac{1}{\delta} \frac{\partial}{\partial y}$. In the FFLW case we will assume that u_j is 1-periodic in y , that is $u_j(x, y) = u_j(x, y + 1)$, while in the FFFW case, we will assume that u_j is 1-antiperiodic, that is $u_j(x, y) = -u_j(x, y + 1)$, see Remark 2.1. In what follows, we will treat both cases simultaneously.

The non-dimensional problem (8)–(9) can hence be rewritten as the governing equation

$$\sum_{j \geq 0} \left[\delta^j \frac{\partial}{\partial y} \left(\beta \frac{\partial u_j}{\partial y} \right) + \delta^{j+1} \left\{ \beta \frac{\partial^2 u_j}{\partial x \partial y} + \frac{\partial}{\partial y} \left(\beta \frac{\partial u_j}{\partial x} \right) \right\} + \delta^{j+2} \beta \frac{\partial^2 u_j}{\partial x^2} + \sum_{\ell \geq 0} \delta^{\ell+j} \mu_\ell^2 \alpha u_j \right] = 0, \quad (13)$$

subject to the jump conditions at $y_n = n$:

$$\sum_{j \geq 0} \delta^j \llbracket u_j(x, y) \rrbracket_{y_n} = \frac{\delta}{\mathcal{K}} \sum_{j \geq 0} \delta^j \left\langle \left\langle \beta(y) \left(\frac{\partial u_j}{\partial x} + \frac{1}{\delta} \frac{\partial u_j}{\partial y} \right) \right\rangle \right\rangle_{y_n}, \quad (14)$$

and

$$\delta \sum_{j \geq 0} \delta^j \left\langle \left\langle \beta(y) \left(\frac{\partial u_j}{\partial x} + \frac{1}{\delta} \frac{\partial u_j}{\partial y} \right) \right\rangle \right\rangle_{y_n} = -m \left(\sum_{\ell \geq 0} \delta^\ell \mu_\ell^2 \right) \left(\sum_{j \geq 0} \delta^j \llbracket u_j \rrbracket_{y_n} \right), \quad (15)$$

where for any function $g(x, y)$, the jump and mean brackets are naturally defined for $n \in \mathbb{Z}$ as

$$\llbracket g(x, y) \rrbracket_{y_n} = g(x, n^+) - g(x, n^-) \quad \text{and} \quad \langle \langle g \rangle \rangle_{y_n} = \frac{1}{2} (g(x, n^+) + g(x, n^-)). \quad (16)$$

Note 2.2. In order for our expansion to be compatible with the assumption regarding potential discontinuities of ρ and E within the unit cell made in Note 2.1, we seek the fields such that u_0 , $\beta \frac{\partial u_0}{\partial y}$, u_j and $\beta \left(\frac{\partial u_j}{\partial y} + \frac{\partial u_{j-1}}{\partial x} \right)$ for $j \geq 1$ are continuous functions of y on $(0, 1)$.

Before pushing the asymptotic analysis further, we need to discuss some important properties of the jump and mean brackets. We will start with a very useful property (that can be proved directly), namely that for any two functions $f(x, y)$ and $g(x, y)$, and any $n \in \mathbb{Z}$, the following relation is valid:

$$\llbracket fg \rrbracket_{y_n} = \llbracket f \rrbracket_{y_n} \langle \langle g \rangle \rangle_{y_n} + \langle \langle f \rangle \rangle_{y_n} \llbracket g \rrbracket_{y_n}. \quad (17)$$

It is equally important to note that if the function subjected to the brackets is either periodic or antiperiodic, the following result holds.

Lemma 2.1. Let $n \in \mathbb{Z}$. If a function $g^{\text{per}}(x, y)$ is 1-periodic in y , then we can write

$$\llbracket g^{\text{per}} \rrbracket_{y_n} = g^{\text{per}}(x, 0^+) - g^{\text{per}}(x, 1^-) \quad \text{and} \quad \langle \langle g^{\text{per}} \rangle \rangle_{y_n} = \frac{1}{2} (g^{\text{per}}(x, 0^+) + g^{\text{per}}(x, 1^-)),$$

while for a function $g^{\text{anti}}(x, y)$ that is 1-antiperiodic in y , we have

$$\llbracket g^{\text{anti}} \rrbracket_{y_n} = g^{\text{anti}}(x, 0^+) + g^{\text{anti}}(x, 1^-) \quad \text{and} \quad \langle \langle g^{\text{anti}} \rangle \rangle_{y_n} = \frac{1}{2} (g^{\text{anti}}(x, 0^+) - g^{\text{anti}}(x, 1^-)).$$

The Lemma 2.1 means that as long as the function subjected to either the jump or the mean bracket is 1-periodic or 1-antiperiodic in y , then the mean and jump brackets values are independent of n , and the y_n subscript can be dropped. Since $\beta(y)$ is 1-periodic and $u_j(x, y)$ is either 1-periodic or 1-antiperiodic in y , this is the case for all the brackets in the conditions (14) and (15), we will hence drop the subscript from now on and just use $\llbracket \cdot \rrbracket$ and $\langle \cdot \rangle$. We will make sure that whenever this notation is used, the function inside the brackets is either periodic or antiperiodic. In particular, from Lemma 2.1 and (17), we obtain directly the following lemma that will prove very important in what follows.

Lemma 2.2. *For any two functions $f(x, y)$ and $g(x, y)$ that are either 1-periodic or 1-antiperiodic in y , we have $\llbracket fg \rrbracket = \llbracket f \rrbracket \langle g \rangle + \langle f \rangle \llbracket g \rrbracket$.*

Finally, in order to link the average operator and the jump bracket, the following result will be very useful.

Lemma 2.3. *For any function $g^{\text{per}}(x, y)$ that is 1-periodic and continuous for $y \in (0, 1)$, we have*

$$\left\langle \frac{\partial g^{\text{per}}}{\partial y} \right\rangle = -\llbracket g^{\text{per}} \rrbracket$$

Notation 2.1. *From now on, in order to efficiently deal with the FFLW (Finite Frequency Low Wavenumber, $\kappa\delta \approx 0$) and the FFFW (Finite Frequency Finite Wavenumber, $\kappa\delta \approx \pi$) cases simultaneously, we will assume that whenever the symbols \pm or \mp are used, the top sign corresponds to FFLW while the bottom sign corresponds to FFFW.*

We are now well equipped to start developing the core theoretical part of the paper.

3. The case of simple eigenvalues

We will now deploy the two-scale asymptotic procedure in order to derive the approximation (2). In order to do so we will need to consider the contributions of (13)–(15) at the orders δ^0 , δ^1 and δ^2 .

3.1. Zeroth-order field

Upon collecting the terms of order δ^0 in (13)–(15), we obtain the system

$$(18a) \quad \frac{\partial}{\partial y} \left(\beta \frac{\partial u_0}{\partial y} \right) + \mu_0^2 \alpha u_0 = 0 \quad \text{with} \quad (18b) \quad \begin{cases} \llbracket u_0 \rrbracket = \frac{1}{\kappa} \langle \beta \frac{\partial u_0}{\partial y} \rangle, \\ \llbracket \beta \frac{\partial u_0}{\partial y} \rrbracket = -m \mu_0^2 \langle u_0 \rangle. \end{cases} \quad (18)$$

Upon considering the (Sturm-Liouville) differential operator $\mathcal{L} := \frac{-1}{\alpha} \frac{d}{dy} \left(\beta \frac{d}{dy} \right)$, one can see that the system (18) constitutes an eigenvalue problem for \mathcal{L} . It is a bit unusual since the eigenvalue also appears in the boundary conditions, but one can show, using the tailored inner product $\langle \cdot, \cdot \rangle$ defined for some functions $f(y)$ and $g(y)$ (either both FFLW or both FFFW) by

$$\langle f, g \rangle = \langle \alpha f \bar{g} \rangle + m \langle \llbracket f \rrbracket \langle \bar{g} \rangle \rangle, \quad (19)$$

that this operator is symmetric (i.e. self-adjoint) and non-negative in both the FFLW and FFFW cases, the proof being deferred to [Appendix A](#). Therefore it has a discrete set of (possibly repeated) real positive eigenvalues associated to real eigenfunctions. We denote the square root

of such eigenvalues by μ_0 , and we note that eigenfunctions associated to different FFLW (resp. FFFW) eigenvalues are orthogonal for the inner product (19). These reduced frequencies μ_0 correspond to the intersection of the dispersion diagram with the left (FFLW) or the right (FFFW) border of the Brillouin zone.

From now on we will choose one of these eigenvalues, denote it by μ_0 , and endeavour to approximate the solutions for some parameters $(\mu, \tilde{\kappa})$ close to $(\mu_0, 0)$, where we define $\tilde{\kappa}$ to be

$$\text{(FFLW)} : \tilde{\kappa} = \kappa \quad \text{and} \quad \text{(FFFW)} : \tilde{\kappa} = \pi/\delta - \kappa, \quad (20)$$

allowing us to treat the FFLW and FFFW cases simultaneously. We will also assume that μ_0 is a simple eigenvalue (multiplicity 1). The case of a double eigenvalue will be dealt with in §4. Hence, there is only one eigenfunction that we denote $\hat{u}_0(y)$ and that is either periodic (FFLW) or antiperiodic (FFFW). The associated solution u_0 to (18) can therefore be rewritten

$$u_0(x, y) = \mathcal{U}_0(x)\hat{u}_0(y), \quad (21)$$

for some function $\mathcal{U}_0(x)$. It is worth mentioning at this stage that when inputting (21) into (18), we find that $\hat{u}_0(y)$ satisfies both the equation (18a) and the jump conditions (18b), a fact that will be used throughout the paper.

The main aim of what follows is to derive a differential equation with constant coefficients satisfied by $\mathcal{U}_0(x)$. Note that in the case of low-frequency homogenisation, the zeroth-order field $u_0(x, y)$ can be shown to be independent of y ; this is one of the main differences between low- and high-frequency homogenisation.

3.2. First-order field

Let us now set μ_0 to be one of the reduced frequencies found in the previous section, we can collect the terms of order δ^1 in (13)–(15) to obtain the following system governing the first-order field u_1 :

$$\frac{\partial}{\partial y} \left(\beta \left(\frac{\partial u_1}{\partial y} + \frac{\partial u_0}{\partial x} \right) \right) + \beta \frac{\partial^2 u_0}{\partial x \partial y} + \alpha(\mu_0^2 u_1 + \mu_1^2 u_0) = 0, \quad (22)$$

subject to the jump conditions

$$\llbracket u_1 \rrbracket = \frac{1}{\tilde{\kappa}} \left\langle \left\langle \beta \left(\frac{\partial u_0}{\partial x} + \frac{\partial u_1}{\partial y} \right) \right\rangle \right\rangle \quad \text{and} \quad \left\langle \left\langle \beta \left(\frac{\partial u_0}{\partial x} + \frac{\partial u_1}{\partial y} \right) \right\rangle \right\rangle = -m(\mu_0^2 \langle u_1 \rangle + \mu_1^2 \langle u_0 \rangle). \quad (23)$$

We will show below that there is only one possible value of μ_1 , and that it has to be zero.

3.2.1. Proving that $\mu_1 = 0$

Following [6], we consider $\langle u_1 \times (18a) - u_0 \times (22) \rangle$. The terms in $\alpha\mu_0^2 u_0 u_1$ cancel out, and using the fact that

$$u_1 \frac{\partial}{\partial y} \left(\beta \frac{\partial u_0}{\partial y} \right) - u_0 \frac{\partial}{\partial y} \left(\beta \left(\frac{\partial u_1}{\partial y} + \frac{\partial u_0}{\partial x} \right) \right) = \frac{\partial}{\partial y} \left(u_1 \beta \frac{\partial u_0}{\partial y} - u_0 \beta \left(\frac{\partial u_1}{\partial y} + \frac{\partial u_0}{\partial x} \right) \right) + \beta \frac{\partial u_0}{\partial y} \frac{\partial u_0}{\partial x},$$

we obtain

$$\left\langle \frac{\partial}{\partial y} \left(u_1 \beta \frac{\partial u_0}{\partial y} - u_0 \beta \left(\frac{\partial u_1}{\partial y} + \frac{\partial u_0}{\partial x} \right) \right) \right\rangle = \underbrace{\left\langle \beta \left(u_0 \frac{\partial^2 u_0}{\partial x \partial y} - \frac{\partial u_0}{\partial x} \frac{\partial u_0}{\partial y} \right) \right\rangle}_{=0} + \mu_1^2 \langle \alpha u_0^2 \rangle. \quad (24)$$

Note that due to the form (21) of u_0 , we have $u_0 \frac{\partial^2 u_0}{\partial x \partial y} - \frac{\partial u_0}{\partial x} \frac{\partial u_0}{\partial y} = 0$, so the first bracket in the right-hand side (RHS) of the equation above is actually zero. Now, using Note 2.2 and Lemma 2.3, (24) becomes

$$-\left[u_1 \beta \frac{\partial u_0}{\partial y} - u_0 \beta \left(\frac{\partial u_1}{\partial y} + \frac{\partial u_0}{\partial x} \right) \right] = \mu_1^2 \langle \alpha u_0^2 \rangle. \quad (25)$$

When perfect interfaces are considered, the jump bracket term in (25) is automatically zero, a fact that is used in [6] to conclude that $\mu_1 = 0$. Such reasoning cannot be used directly in our case. Instead, make use of Lemma 2.2 to rewrite (25) as

$$\begin{aligned} \mu_1^2 \langle \alpha u_0^2 \rangle &= -\llbracket u_1 \rrbracket \left\langle \left\langle \beta \frac{\partial u_0}{\partial y} \right\rangle \right\rangle - \langle u_1 \rangle \left[\left[\beta \frac{\partial u_0}{\partial y} \right] + \llbracket u_0 \rrbracket \left\langle \left\langle \beta \left(\frac{\partial u_1}{\partial y} + \frac{\partial u_0}{\partial x} \right) \right\rangle \right\rangle + \langle u_0 \rangle \left[\left[\beta \left(\frac{\partial u_1}{\partial y} + \frac{\partial u_0}{\partial x} \right) \right] \right] \right. \\ &= -\cancel{\llbracket u_0 \rrbracket \llbracket u_1 \rrbracket} + m \mu_0^2 \langle u_1 \rangle \langle u_0 \rangle + \cancel{\llbracket u_0 \rrbracket \llbracket u_1 \rrbracket} - m \langle u_0 \rangle (\mu_0^2 \langle u_1 \rangle + \mu_1^2 \langle u_0 \rangle), \end{aligned} \quad (26)$$

where the jump conditions (18a) and (23) have been used. Many terms cancel out and we get

$$\mu_1^2 (\langle \alpha u_0^2 \rangle + m \langle u_0 \rangle^2) = 0, \quad \text{implying that} \quad \mu_1 = 0, \quad (27)$$

because m and α are strictly positive, and, in the representation (21), \mathcal{U}_0 cannot be identically zero and \hat{u}_0 is a real function. This result is very important and lies at the heart of the success of the high-frequency homogenisation method.

3.2.2. An expression for $u_1(x, y)$

We can now simplify the equation (22) governing u_1 to

$$\frac{\partial}{\partial y} \left(\beta \frac{\partial u_1}{\partial y} \right) + \alpha \mu_0^2 u_1 = -\mathcal{U}'_0(x) (2\beta(y) \hat{u}'_0(y) + \beta'(y) \hat{u}_0(y)). \quad (28)$$

Upon noting that, because \hat{u}_0 is solution to (18a), the field $-y \mathcal{U}'_0(x) \hat{u}_0(y)$ is a particular solution to (28), and that the differential operator applied to u_1 is exactly the same as that of (18a), we can conclude that u_1 can be written as

$$u_1(x, y) = \mathcal{U}_1(x) \hat{u}_0(y) + \mathcal{V}'_0(x) (v_1(y) - y \hat{u}_0(y)), \quad (29)$$

for some function $\mathcal{U}_1(x)$ that will be shown not to play any role in what follows, and a function $v_1(y)$, that is another solution to (18a), independent of $\hat{u}_0(y)$, and that is chosen to ensure that the jump conditions

$$\llbracket u_1 \rrbracket = \frac{1}{\cancel{\beta}} \left\langle \left\langle \beta \left(\frac{\partial u_0}{\partial x} + \frac{\partial u_1}{\partial y} \right) \right\rangle \right\rangle \quad \text{and} \quad \left[\left[\beta \left(\frac{\partial u_0}{\partial x} + \frac{\partial u_1}{\partial y} \right) \right] \right] = -m \mu_0^2 \langle u_1 \rangle \quad (30)$$

are satisfied. These jump conditions come from (23), where we have used that $\mu_1 = 0$. Note that because of (29), and the periodicity properties of u_1 and \hat{u}_0 , the function $v_1(y) - y \hat{u}_0(y)$ has to be periodic (FFLW) or antiperiodic (FFFW). Because this function will appear many times in what follows, it is worth giving it a name. Hence, we define

$$f_1(y) \stackrel{\text{def}}{=} v_1(y) - y \hat{u}_0(y). \quad (31)$$

Inputting the form (29) into (30), leads to two conditions on f_1 :

$$\llbracket f_1 \rrbracket = \frac{1}{\hbar} \langle\langle \beta f_1' \rangle\rangle + \frac{1}{\hbar} \langle\langle \beta \hat{u}_0 \rangle\rangle, \quad (32)$$

$$-m\mu_0^2 \langle\langle f_1 \rangle\rangle = \llbracket \beta f_1' \rrbracket + \llbracket \beta \hat{u}_0 \rrbracket. \quad (33)$$

One should notice, in particular, that no terms involving $\mathcal{U}_1(x)$ appear in these conditions.

Remark 3.1. For practical computations of the function $v_1(y)$, which are required when dealing with specific examples, we can use Lemma 2.1 to rewrite the two jump conditions (32) and (33) as

$$\mathcal{L}_1[v_1] = \mathcal{K}_1[\hat{u}_0] \quad \text{and} \quad \mathcal{L}_2[v_1] = \mathcal{K}_2[\hat{u}_0],$$

where

$$\mathcal{L}_1[v_1] = v_1(0^+) \mp v_1(1^-) - \frac{1}{2\hbar} (\beta(0^+)v_1'(0^+) \pm \beta(1^-)v_1'(1^-)),$$

$$\mathcal{K}_1[\hat{u}_0] = \mp \hat{u}_0(1^-) \mp \frac{1}{2\hbar} \beta(1^-) \hat{u}_0'(1^-),$$

$$\mathcal{L}_2[v_1] = -\frac{m\mu_0^2}{2} (v_1(0^+) \pm v_1(1^-)) - (\beta(0^+)v_1'(0^+) \mp \beta(1^-)v_1'(1^-)),$$

$$\mathcal{K}_2[\hat{u}_0] = \mp \frac{m\mu_0^2}{2} \hat{u}_0(1^-) \pm \beta(1^-) \hat{u}_0'(1^-),$$

where Notation 2.1 has been used. Note that $\mathcal{L}_{1,2}$ are the same operators as those applied to \hat{u}_0 when determining μ_0 , though in this case the right-hand side was 0. Here we have these non-zero $\mathcal{K}_{1,2}$ terms.

3.3. Second-order field

We can now collect the terms of order δ^2 in (13)–(15) to obtain the following equation governing the second-order field u_2 :

$$\frac{\partial}{\partial y} \left(\beta \left(\frac{\partial u_2}{\partial y} + \frac{\partial u_1}{\partial x} \right) \right) + \mu_0^2 \alpha u_2 + \beta \frac{\partial^2 u_1}{\partial x \partial y} + \beta \frac{\partial^2 u_0}{\partial x^2} + \mu_2^2 \alpha u_0 = 0, \quad (34)$$

subject to the jump conditions

$$\llbracket u_2 \rrbracket = \frac{1}{\hbar} \langle\langle \beta \left(\frac{\partial u_2}{\partial y} + \frac{\partial u_1}{\partial x} \right) \rangle\rangle \quad \text{and} \quad \llbracket \beta \left(\frac{\partial u_2}{\partial y} + \frac{\partial u_1}{\partial x} \right) \rrbracket = -m(\mu_0^2 \langle\langle u_2 \rangle\rangle + \mu_2^2 \langle\langle u_0 \rangle\rangle). \quad (35)$$

Similarly to §3(b)3.2.1, we consider the quantity $\langle u_2 \times (18a) - u_0 \times (34) \rangle$. The terms in $\alpha \mu_0^2 u_0 u_2$ cancel out, and, using the fact that

$$u_2 \frac{\partial}{\partial y} \left(\beta \frac{\partial u_0}{\partial y} \right) - u_0 \frac{\partial}{\partial y} \left(\beta \left(\frac{\partial u_2}{\partial y} + \frac{\partial u_1}{\partial x} \right) \right) = \frac{\partial}{\partial y} \left(u_2 \beta \frac{\partial u_0}{\partial y} - u_0 \beta \left(\frac{\partial u_2}{\partial y} + \frac{\partial u_1}{\partial x} \right) \right) + \beta \frac{\partial u_0}{\partial y} \frac{\partial u_1}{\partial x},$$

we obtain

$$\left\langle \frac{\partial}{\partial y} \left(u_2 \beta \frac{\partial u_0}{\partial y} - u_0 \beta \left(\frac{\partial u_2}{\partial y} + \frac{\partial u_1}{\partial x} \right) \right) \right\rangle = \left\langle \beta \left(u_0 \frac{\partial^2 u_1}{\partial x \partial y} - \frac{\partial u_0}{\partial y} \frac{\partial u_1}{\partial x} + u_0 \frac{\partial^2 u_0}{\partial x^2} \right) \right\rangle + \mu_2^2 \langle \alpha u_0^2 \rangle. \quad (36)$$

Now, note that, by directly using (21), (29) and (31) we can show that

$$u_0 \frac{\partial^2 u_1}{\partial x \partial y} - \frac{\partial u_0}{\partial y} \frac{\partial u_1}{\partial x} + u_0 \frac{\partial^2 u_0}{\partial x^2} = \mathcal{U}_0(x) \mathcal{U}_0''(x) w_1(y), \quad (37)$$

where we define

$$w_1 \stackrel{\text{def}}{=} \hat{u}_0 f_1' - \hat{u}_0' f_1 + (\hat{u}_0)^2. \quad (38)$$

Moreover, the first bracket of (36) can be simplified using using Note 2.2 and Lemma 2.3 and, therefore, using (37), (36) becomes

$$- \left[u_2 \beta \frac{\partial u_0}{\partial y} - u_0 \beta \left(\frac{\partial u_2}{\partial y} + \frac{\partial u_1}{\partial x} \right) \right] = \mathcal{U}_0(x) \mathcal{U}_0''(x) \langle \beta w_1 \rangle + \mu_2^2 \langle \alpha u_0^2 \rangle. \quad (39)$$

Remark 3.2. Inputting (31) into (38), one shows that $w_1 = \hat{u}_0 v_1' - \hat{u}_0' v_1$, which is the Wronskian associated to the second-order ODE $(\beta g')' + \mu_0^2 \alpha g = 0$, and hence satisfies the first-order ODE $(\beta w_1)' = 0$. Moreover, the hypothesis made in Note 2.2 regarding potential material properties discontinuities within the interior of the unit cell implies that \hat{u}_0 , $\beta \hat{u}_0'$, u_1 and $\beta \left(\frac{\partial u_1}{\partial y} + \mathcal{U}_0'(x) \hat{u}_0 \right)$ are continuous in y on $(0, 1)$. Using the form (29) of u_1 , this implies that both v_1 and $\beta v_1'$ should be continuous on $(0, 1)$, and hence that βw_1 is continuous on $(0, 1)$, which, using the fact that $(\beta w_1)' = 0$, implies that βw_1 is constant on $(0, 1)$. Therefore $\langle \beta w_1 \rangle = \beta(0^+) w_1(0^+)$ say, and its computation does not require any integration. Moreover, since \hat{u}_0 and v_1 are independent, it is clear that $\langle \beta w_1 \rangle \neq 0$.

As in §3.2.1, we can now make use of Lemma 2.2 to simplify the left-hand side (LHS) of (39):

$$\begin{aligned} - \left[u_2 \beta \frac{\partial u_0}{\partial y} - u_0 \beta \left(\frac{\partial u_2}{\partial y} + \frac{\partial u_1}{\partial x} \right) \right] &= - \llbracket u_2 \rrbracket \left\langle \left\langle \beta \frac{\partial u_0}{\partial y} \right\rangle \right\rangle - \langle u_2 \rangle \left[\left[\beta \frac{\partial u_0}{\partial y} \right] \right] + \llbracket u_0 \rrbracket \left\langle \left\langle \beta \left(\frac{\partial u_2}{\partial y} + \frac{\partial u_1}{\partial x} \right) \right\rangle \right\rangle \\ &\quad + \langle u_0 \rangle \left[\left[\beta \left(\frac{\partial u_2}{\partial y} + \frac{\partial u_1}{\partial x} \right) \right] \right] \\ &= - \mathcal{K} \llbracket u_2 \rrbracket \llbracket u_0 \rrbracket + m \mu_0^2 \langle u_2 \rangle \langle u_0 \rangle + \mathcal{K} \llbracket u_0 \rrbracket \llbracket u_2 \rrbracket \\ &\quad - m \langle u_0 \rangle (\mu_0^2 \langle u_2 \rangle + \mu_2^2 \langle u_0 \rangle) = -m \mu_2^2 \langle u_0 \rangle^2, \quad (40) \end{aligned}$$

where the jump conditions (18b) and (35) have been used. Finally, using (40) and dividing through by $\mathcal{U}_0(x)$, (39) can be rewritten as

$$T \mathcal{U}_0''(x) + \mu_2^2 \mathcal{U}_0(x) = 0, \quad \text{where} \quad T = \frac{\langle \beta w_1 \rangle}{\langle \alpha (\hat{u}_0)^2 \rangle + m \langle \hat{u}_0 \rangle^2}, \quad (41)$$

which is the effective equation for \mathcal{U}_0 .

3.4. Approximation of the dispersion branches

Note that in (41) $T \neq 0$, but it can be either negative or positive. Since we are looking for standing waves, we seek μ_2^2 such that $\mu_2^2/T \geq 0$. Remember that μ_2 is a correction term to the reduced frequency μ , such that $\mu^2 = \mu_0^2 + \delta^2 \mu_2^2 + o(\delta^2)$. This means that for each branch of the

dispersion diagram (determined by our initial choice of eigenvalue μ_0), we look for a function $\mu_2(\kappa)$ that will lead to an approximation of $\mu(\kappa)$ at the second order in δ , where κ is the reduced Bloch wavenumber. In particular, by definition of the FFLW and FFFW cases, we should have

$$\text{(FFLW)} \quad \mu_2(\kappa) \xrightarrow{\kappa \rightarrow 0} 0 \quad \text{and} \quad \text{(FFFW)} \quad \mu_2(\kappa) \xrightarrow{\kappa \rightarrow \frac{\pi}{\delta}} 0. \quad (42)$$

In order for our asymptotic representation (12) to be compatible with the fact that u_δ should satisfy the Bloch-Floquet conditions (11), it is enough to impose that all the $u_j(x, \frac{x}{\delta})$ should also satisfy these conditions. For $j = 0$, this means that

$$\mathcal{U}_0(x + \delta)\hat{u}_0\left(\frac{x}{\delta} + 1\right) = \mathcal{U}_0(x)\hat{u}_0\left(\frac{x}{\delta}\right)e^{i\kappa\delta}. \quad (43)$$

Hence, due to fact that \hat{u}_0 is periodic (FFLW) or antiperiodic (FFFW), we can cancel out the terms in \hat{u}_0 in (43) to get

$$\mathcal{U}_0(x + \delta) = \pm \mathcal{U}_0(x)e^{i\kappa\delta}, \quad (44)$$

where, in (44) and below, Notation 2.1 is being used. The second Bloch-Floquet condition in (11), combined with (44), implies that

$$\mathcal{U}'_0(x + \delta) = \pm \mathcal{U}'_0(x)e^{i\kappa\delta}. \quad (45)$$

Because \mathcal{U}_0 is solution to (41), it can be written $\mathcal{U}_0(x) = Ae^{i\sqrt{\mu_2^2/T}x} + Be^{-i\sqrt{\mu_2^2/T}x}$ for some constants A and B . The Bloch-Floquet conditions (44) and (45) lead to

$$A\left(1 \mp e^{i\delta(\sqrt{\mu_2^2/T} - \kappa)}\right) = 0 \quad \text{and} \quad B\left(1 \mp e^{-i\delta(\sqrt{\mu_2^2/T} + \kappa)}\right) = 0. \quad (46)$$

Since κ is restricted to $(0, \frac{\pi}{\delta})$, i.e. to the first Brillouin zone in the dispersion diagram, and since it is assumed that $\mu_2^2/T \geq 0$, (46) implies that, using (20), we have

$$\sqrt{\mu_2^2/T} = \tilde{\kappa} \quad \text{and} \quad \mathcal{U}_0(x) = e^{\pm i\tilde{\kappa}x}, \quad (47)$$

which gives the following approximation for the reduced frequency $\mu(\kappa)$

$$\mu^2 = \mu_0^2 + T(\tilde{\kappa}\delta)^2 + o(\tilde{\kappa}^2\delta^2) \quad \text{or equivalently} \quad \mu = \mu_0 + \frac{T}{2\mu_0}(\tilde{\kappa}\delta)^2 + o(\tilde{\kappa}^2\delta^2). \quad (48)$$

The non-dimensional wave field is approximated by

$$u_\delta(x) = \underbrace{\mathcal{U}_0(x)\hat{u}_0(x/\delta)}_{u_0(x, x/\delta)} + O(\tilde{\kappa}\delta) \quad (49)$$

Note that in §6, we will find it more convenient to test the validity of (49) when it is written in terms of the variable y as follows

$$u_\delta(\delta y) = \underbrace{\mathcal{U}_0(\delta y)\hat{u}_0(y)}_{u_0(\delta y, y)} + O(\tilde{\kappa}\delta) \quad (50)$$

Hence, as anticipated, using (7), our results can be summarised in dimensional form by (2) and (3), where the parameter \mathcal{T} and the leading-order wave field $U_h^{(0)}$ are given by

$$\mathcal{T} = \frac{(c^*)^2}{h^2}T, \quad \omega_0 = \frac{c^*\mu_0}{h} \quad \text{and} \quad U_h^{(0)}(X) = e^{\pm i\tilde{\kappa}X}\hat{u}_0(X/h).$$

4. The case of a double eigenvalue μ_0

4.1. A new form for u_0

In order to write (21), we assumed that μ_0 was a simple eigenvalue. If instead we assume that μ_0 has multiplicity 2 say, then we write

$$u_0(x, y) = \underbrace{\mathcal{U}_0^{(1)}(x)\hat{u}_0^{(1)}(y)}_{u_0^{(1)}(x,y)} + \underbrace{\mathcal{U}_0^{(2)}(x)\hat{u}_0^{(2)}(y)}_{u_0^{(2)}(x,y)}, \quad (51)$$

where $\hat{u}_0^{(1)}(y)$ and $\hat{u}_0^{(2)}(y)$ are two independent eigenfunctions associated to the double eigenvalue μ_0 and $\mathcal{U}_0^{(1)}(x)$ and $\mathcal{U}_0^{(2)}(x)$ are some functions of x to be determined. Note that both $\hat{u}_0^{(1)}(y)$ and $\hat{u}_0^{(2)}(y)$ satisfy (18a)–(18b). In what follows, for any $j \in \{1, 2\}$, we will use the notation (18a)^(j) and (18b)^(j), to specify that we consider (18a)–(18b) as applied to $\hat{u}_0^{(j)}(y)$.

4.2. In this case, we cannot conclude that $\mu_1 = 0$

We will now apply the same methodology as in §3.2.1 and consider the quantity $\langle u_1 \times (18a)^{(1)} - u_0^{(1)} \times (22) \rangle$. The exact same reasoning leads to the counterpart to (24):

$$\left\langle \frac{\partial}{\partial y} \left(u_1 \beta \frac{\partial u_0^{(1)}}{\partial y} - u_0^{(1)} \beta \left(\frac{\partial u_1}{\partial y} + \frac{\partial u_0}{\partial x} \right) \right) \right\rangle = \left\langle \beta \left(u_0^{(1)} \frac{\partial^2 u_0}{\partial x \partial y} - \frac{\partial u_0}{\partial x} \frac{\partial u_0^{(1)}}{\partial y} \right) \right\rangle + \mu_1^2 \langle \alpha u_0^{(1)} u_0 \rangle. \quad (52)$$

The only difference being that this time, the first bracket in the RHS of (52) is not zero. Instead, it can be shown directly using (51) that

$$u_0^{(1)} \frac{\partial^2 u_0}{\partial x \partial y} - \frac{\partial u_0}{\partial x} \frac{\partial u_0^{(1)}}{\partial y} = \mathcal{U}_0^{(1)}(x) \mathcal{U}_0^{(2)'}(x) w_0(y), \quad (53)$$

where w_0 is the Wronskian defined by

$$w_0(y) = \hat{u}_0^{(1)}(y) \hat{u}_0^{(2)'}(y) - \hat{u}_0^{(1)'}(y) \hat{u}_0^{(2)}(y). \quad (54)$$

The same methodology to simplify the LHS bracket in (52) as that used in §3.2.1 can be used: first use Lemma 2.3 to reduce the average bracket to a jump bracket, then use Lemma 2.2 to decompose the jump bracket into four simpler jump/mean brackets that can be computed using the jump conditions (18b)⁽¹⁾ and (23) to obtain

$$-m \mu_1^2 \langle u_0^{(1)} \rangle \langle u_0 \rangle = \mathcal{U}_0^{(1)}(x) \mathcal{U}_0^{(2)'}(x) \langle \beta w_0 \rangle + \mu_1^2 \langle \alpha u_0^{(1)} u_0 \rangle, \quad (55)$$

which, upon regrouping the terms, dividing through by $\mathcal{U}_0^{(1)}(x)$ and using (51), can be rewritten

$$\langle \beta w_0 \rangle \mathcal{U}_0^{(2)'}(x) = -\mu_1^2 \left(\{m B_1^2 + C_1\} \mathcal{U}_0^{(1)}(x) + \{m B_1 B_2 + D\} \mathcal{U}_0^{(2)}(x) \right), \quad (56)$$

where we have defined

$$B_1 = \langle \hat{u}_0^{(1)} \rangle, \quad B_2 = \langle \hat{u}_0^{(2)} \rangle, \quad C_1 = \langle \alpha (\hat{u}_0^{(1)})^2 \rangle, \quad C_2 = \langle \alpha (\hat{u}_0^{(2)})^2 \rangle, \quad D = \langle \alpha \hat{u}_0^{(1)} \hat{u}_0^{(2)} \rangle. \quad (57)$$

In the exact same way, we consider the quantity $\langle u_1 \times (18a)^{(2)} - u_0^{(2)} \times (22) \rangle$ to obtain

$$\langle \beta w_0 \rangle \mathcal{U}_0^{(1)'}(x) = \mu_1^2 \left(\{m B_1 B_2 + D\} \mathcal{U}_0^{(1)}(x) + \{m B_2^2 + C_2\} \mathcal{U}_0^{(2)}(x) \right). \quad (58)$$

Note that w_0 is the Wronskian determinant associated to (18a), and βw_0 can be shown to be continuous on the unit cell, hence we conclude that βw_0 is actually constant, and hence we can see that $\langle \beta w_0 \rangle = \beta(0^+) w_0(0^+)$. Since $\hat{u}_0^{(1)}$ and $\hat{u}_0^{(2)}$ are linearly independent, w_0 (being the associated Wronskian) is also non-zero and in this case, we cannot conclude that $\mu_1 = 0$.

4.3. Solving a first-order ODE system to obtain μ_1

Upon introducing the function vector $\mathbf{U} = (\mathbf{U}_0^{(1)}, \mathbf{U}_0^{(2)})^T$, the two equations (56) and (58) can be recast as the first-order ODE system

$$\mathbf{U}'(x) = \frac{\mu_1^2}{\langle \beta \mathbf{w}_0 \rangle} \mathcal{N} \mathbf{U}(x), \quad \text{where} \quad \mathcal{N} = \begin{pmatrix} mB_1B_2 + D & mB_2^2 + C_2 \\ -(mB_1^2 + C_1) & -(mB_1B_2 + D) \end{pmatrix}. \quad (59)$$

The two eigenvalues $\lambda_{1,2}$ of \mathcal{N} are given by

$$\lambda_j = i(-1)^j \sqrt{(mB_1^2 + C_1)(mB_2^2 + C_2) - (mB_1B_2 + D)^2}, \quad (60)$$

where, by the Cauchy-Schwarz inequality associated to the inner product (19), the quantity inside the square root is positive. The associated eigenvectors are given by

$$\mathbf{u}_{\lambda_1} = \left(\frac{-(mB_1B_2 + D) + \lambda_2}{mB_1^2 + C_1}, 1 \right)^T \quad \text{and} \quad \mathbf{u}_{\lambda_2} = \left(\frac{-(mB_1B_2 + D) + \lambda_1}{mB_1^2 + C_1}, 1 \right)^T \quad (61)$$

and hence, upon introducing T_d to be

$$T_d = \langle \beta \mathbf{w}_0 \rangle / \sqrt{(mB_1^2 + C_1)(mB_2^2 + C_2) - (mB_1B_2 + D)^2}, \quad (62)$$

the solution to (59) can be written as

$$\mathbf{U}(x) = c_1 \mathbf{u}_{\lambda_1} e^{\frac{\mu_1^2}{\langle \beta \mathbf{w}_0 \rangle} \lambda_1 x} + c_2 \mathbf{u}_{\lambda_2} e^{\frac{\mu_1^2}{\langle \beta \mathbf{w}_0 \rangle} \lambda_2 x} = c_1 \mathbf{u}_{\lambda_1} e^{-i \frac{\mu_1^2}{T_d} x} + c_2 \mathbf{u}_{\lambda_2} e^{i \frac{\mu_1^2}{T_d} x}, \quad (63)$$

for some constants $c_{1,2}$. At this stage, we need to remember the Bloch-Floquet conditions (11), which, when applied to u_0 , imply that

$$\hat{u}_0^{(1)}(y) \{ \pm \mathbf{U}_0^{(1)}(x + \delta) - e^{ik\delta} \mathbf{U}_0^{(1)}(x) \} + \hat{u}_0^{(2)}(y) \{ \pm \mathbf{U}_0^{(2)}(x + \delta) - e^{ik\delta} \mathbf{U}_0^{(2)}(x) \} = 0,$$

where Notation 2.1 has been used. Since $\hat{u}_0^{(1)}$ and $\hat{u}_0^{(2)}$ are linearly independent, this implies that $\pm \mathbf{U}(x + \delta) = e^{ik\delta} \mathbf{U}(x)$. Applying this condition to (63), leads to the value of μ_1^2 as follows

$$\delta \mu_1^2 = +T_d \tilde{k} \delta \quad \text{or} \quad \delta \mu_1^2 = -T_d \tilde{k} \delta. \quad (64)$$

Hence, since $\mu^2 = \mu_0^2 + \delta \mu_1^2 + o(\delta)$, we obtain the linear approximations

$$\mu = \mu_0 \pm \frac{T_d}{2\mu_0} (\tilde{k} \delta) + o(\tilde{k} \delta). \quad (65)$$

Here, the symbol \pm should not be understood as per Notation 2.1, but as two different slopes, so that, near each double eigenvalue μ_0 of the dispersion diagram, we have two linear approximations with opposite slopes emerging from μ_0 . Such behaviour of the dispersion diagram, is that of so-called Dirac points.

5. The case of two nearby eigenvalues

In what has been done above, there is no uniform transition from the simple eigenvalue case to the double eigenvalue case. As will be seen in the examples of §6, when two simple eigenvalues are close to each other, the agreement between the dispersion diagram and the asymptotic of §3 is somewhat short-lived. In order to remedy to this issue, following some ideas developed in [7, 28], we will derive an asymptotic expansion for two nearby eigenvalues.

Let us assume that we have two nearby eigenvalues $\mu_0^{(1)}$ and $\mu_0^{(2)}$ with their associated eigenfunctions $\hat{u}_0^{(1)}(y)$ and $\hat{u}_0^{(2)}(y)$ that solve (18a)–(18b) and such that $\mu_0^{(1)} < \mu_0^{(2)}$. Since we are seeking an approximation that remains valid when two eigenvalues merge into one, we assume that $\mu_0^{(1,2)}$ both belong to the same side of the dispersion diagram, i.e. they are either both FFLW or both FFFW. Their proximity is characterised by a positive parameter $\gamma = O(1)$ defined by

$$\delta\gamma = (\mu_0^{(2)})^2 - (\mu_0^{(1)})^2. \quad (66)$$

In the vicinity of these eigenvalues we seek expansions of the form (12), in which we choose $\mu_0 = \mu_0^{(1)}$. In order to consider the competing nature of the two eigenvalues, we seek u_0 in the form (51), introducing the functions $\mathcal{U}_0^{(1,2)}(x)$ and $u_0^{(1,2)}(x, y)$ accordingly. With such choice of u_0 , one can show directly that we have

$$\frac{\partial}{\partial y} \left(\beta \frac{\partial u_0}{\partial y} \right) + (\mu_0^{(1)})^2 \alpha u_0 = -\delta\gamma \alpha u_0^{(2)} \quad \text{with} \quad \begin{cases} \llbracket u_0 \rrbracket = \frac{1}{\varepsilon} \left\langle \left\langle \beta \frac{\partial u_0}{\partial y} \right\rangle \right\rangle \\ \llbracket \beta \frac{\partial u_0}{\partial y} \rrbracket = -m(\mu_0^{(1)})^2 \langle u_0 \rangle - m\delta\gamma \langle u_0^{(2)} \rangle \end{cases} \quad (67)$$

The terms involving δ in the right-hand sides of (67) should be considered when collecting the terms of order δ in (13)–(15) to obtain the equation governing u_1 :

$$\frac{\partial}{\partial y} \left(\beta \left(\frac{\partial u_1}{\partial y} + \frac{\partial u_0}{\partial x} \right) \right) + \beta \frac{\partial^2 u_0}{\partial x \partial y} + \alpha \left((\mu_0^{(1)})^2 u_1 + \mu_1^2 u_0 - \gamma u_0^{(2)} \right) = 0, \quad (68)$$

and the associated jump conditions

$$\llbracket u_1 \rrbracket = \frac{1}{\varepsilon} \left\langle \left\langle \beta \left(\frac{\partial u_0}{\partial x} + \frac{\partial u_1}{\partial y} \right) \right\rangle \right\rangle \quad \text{and} \quad \llbracket \beta \left(\frac{\partial u_0}{\partial x} + \frac{\partial u_1}{\partial y} \right) \rrbracket = -m((\mu_0^{(1)})^2 \langle u_1 \rangle + \mu_1^2 \langle u_0 \rangle - \gamma \langle u_0^{(2)} \rangle). \quad (69)$$

After following the exact same strategy as in §4, consider first the term $\langle u_1 \times (3.1a)^{(1)} - u_0^{(1)} \times (68) \rangle$, and then the term $\langle u_1 \times (3.1a)^{(2)} - u_0^{(2)} \times (68) \rangle$, to obtain two equations that can be recast in the first-order ODE system

$$\mathcal{U}'(x) = \frac{\mu_1^2}{\langle \beta w_0 \rangle} \mathcal{N}_\gamma \mathcal{U}(x). \quad (70)$$

Here we used $\mathcal{U} = (\mathcal{U}_0^{(1)}, \mathcal{U}_0^{(2)})^T$, the function w_0 is defined as in (54) and \mathcal{N}_γ is given by

$$\mathcal{N}_\gamma = \begin{pmatrix} mB_1B_2 + D & \left(1 - \frac{\gamma}{\mu_1^2}\right)(mB_2^2 + C_2) \\ -(mB_1^2 + C_1) & -\left(1 - \frac{\gamma}{\mu_1^2}\right)(mB_1B_2 + D) \end{pmatrix} = \mathcal{N} + \frac{\gamma}{\mu_1^2} \begin{pmatrix} 0 & -mB_2^2 - C_2 \\ 0 & mB_1B_2 + D \end{pmatrix}, \quad (71)$$

the parameters $B_{1,2}$, $C_{1,2}$ and D being defined as in (57). Note that when taking $\gamma \rightarrow 0$ in (70), we recover exactly (59), showing the consistency of our approach. Note that when deriving the second line of (70), we neglect the term $\delta\gamma\langle u_1, \hat{u}_0^{(2)} \rangle$ that occurs in the process since it is of order δ . The eigenvalues $\lambda_{1,2}^{(\gamma)}$ of \mathcal{N}_γ can be found to be given by

$$\lambda_j^{(\gamma)} = \frac{(mB_1B_2 + D)\gamma + (-1)^j \sqrt{(mB_1B_2 + D)^2(\gamma - 2\mu_1^2)^2 + 4(mB_1^2 + C_1)(mB_2^2 + C_2)\mu_1^2(\gamma - \mu_1^2)}}{2\mu_1^2},$$

while the associated eigenvectors are

$$\mathbf{u}_{\lambda_1^{(\gamma)}} = \left(\frac{-(mB_1B_2 + D) + \lambda_2^{(\gamma)}}{(mB_1^2 + C_1)}, 1 \right)^T \quad \text{and} \quad \mathbf{u}_{\lambda_2^{(\gamma)}} = \left(\frac{-(mB_1B_2 + D) + \lambda_1^{(\gamma)}}{(mB_1^2 + C_1)}, 1 \right)^T. \quad (72)$$

We can hence follow what we have done in §4.3, and use the Bloch-Floquet conditions to obtain

$$\text{(FFLW)} : \frac{\mu_1^2 \lambda_j^{(\gamma)}}{\langle \beta_{\mathbf{w}_0} \rangle} = i\kappa \quad \text{and} \quad \text{(FFFW)} : \frac{\mu_1^2 \lambda_j^{(\gamma)}}{\langle \beta_{\mathbf{w}_0} \rangle} = -i \left(\frac{\pi}{\delta} - \kappa \right),$$

which are implicit relationships between μ_1^2 and κ . Fortunately, these can be inverted exactly to obtain

$$\mu_1^2 = \frac{1}{2} \left(\gamma \mp \sqrt{4T_d^2 \tilde{\kappa}^2 + 4iT_d^2 \frac{(mB_1B_2 + D)}{\langle \beta_{\mathbf{w}_0} \rangle} \tilde{\kappa} \gamma + \gamma^2} \right), \quad (73)$$

where (20) has been used, and where T_d is defined as in (62). Here \mp should not be understood as per Notation 2.1, but as two different branches. One issue with (73) is that, in its current form, it implies that μ_1^2 is actually complex. However, this issue is settled by realising that upon using the inner product defined in (19), we can write

$$mB_1B_2 + D = \langle \hat{u}_0^{(1)}, \hat{u}_0^{(2)} \rangle.$$

Hence, since $\hat{u}_0^{(1,2)}$ correspond to two different eigenvalues, they are orthogonal and we get $mB_1B_2 + D = 0$. Therefore, the complex part of (73) disappears and it simplifies to

$$\delta\mu_1^2 = \frac{1}{2} \left(\delta\gamma \mp \sqrt{4T_d^2 (\tilde{\kappa}\delta)^2 + (\delta\gamma)^2} \right) \quad \text{and} \quad \mu^2 = (\mu_0^{(1)})^2 + \delta\mu_1^2 + o(\delta). \quad (74)$$

In the limit $\gamma \rightarrow \infty$ or $\tilde{\kappa} \rightarrow 0$, μ_1^2 behaves like $\mu_1^2 \rightarrow 0$ or $\mu_1^2 \sim \gamma$, depending on the sign chosen in (73). This allows us to conclude that the $-$ sign corresponds to the branch emanating from $\mu_0^{(1)}$, while the $+$ sign corresponds to the branch emanating from $\mu_0^{(2)}$. There are two other interesting limits to consider.

The first is to see what happens when two eigenvalues are merging, i.e., we fix $\tilde{\kappa}\delta$ and let $\delta\gamma \rightarrow 0$. In this case (74) simplifies to $\mu^2 \approx (\mu_0^{(1)})^2 + \frac{\delta\gamma}{2} \mp T_d \tilde{\kappa}\delta$, which, when plotted against $\tilde{\kappa}\delta$ are two straight lines with opposite slopes emanating from a point between the two nearby eigenvalues. When the two eigenvalues merge (i.e. $\delta\gamma = 0$), we recover exactly the double eigenvalue approximation (64).

The second is to see how well (74) approximates the dispersion diagram at the edges of the Brillouin zone for a given $\delta\gamma \neq 0$. So we fix $\delta\gamma$ and let $\tilde{\kappa}\delta \rightarrow 0$. In this case, (74) simplifies to

$$\mu^2 \approx (\mu_0^{(1)})^2 + \frac{1}{2}(\delta\gamma \mp \delta\gamma) \mp \frac{T_d^2}{\delta\gamma}(\tilde{\kappa}\delta)^2.$$

Hence, for the lower branch it becomes $\mu^2 \approx (\mu_0^{(1)})^2 - \frac{T_d^2}{\delta\gamma}(\tilde{\kappa}\delta)^2$, while for the upper branch, it reads $\mu^2 \approx (\mu_0^{(2)})^2 + \frac{T_d^2}{\delta\gamma}(\tilde{\kappa}\delta)^2$. This approximation resembles (48), but with an incorrect quadratic coefficient (since in general $\mp \frac{T_d^2}{\delta\gamma} \neq T$), so it is only a first-order approximation, slightly less precise than the simple eigenvalue approximation.

Hence, (74) is a *uniform approximation*, in the sense that it is valid for both simple and double eigenvalues. Moreover, we will see in the next section that using (74) leads to a much longer-lived fit to the exact dispersion diagram than the simple eigenvalue method.

6. Examples and numerical experiments

The theory developed above has the advantage to be valid for any spatially varying periodic material properties, even in cases when the dispersion diagram cannot be obtained analytically or is computationally intricate to obtain. However, in order to validate the method, we now consider two simpler examples, for which the dispersion diagram can be obtained directly by the Bloch-Floquet analysis.

6.1. Monolayer

The simplest example that can be considered is the case of a monolayer material with imperfect interface. By this we mean that the density and Young's modulus are constant, so that $\rho_h(X) = \rho^*$ and $E_h(X) = E^*$. This implies that $\alpha = \beta = 1$. The geometry of the physical problem is represented in Figure 2.

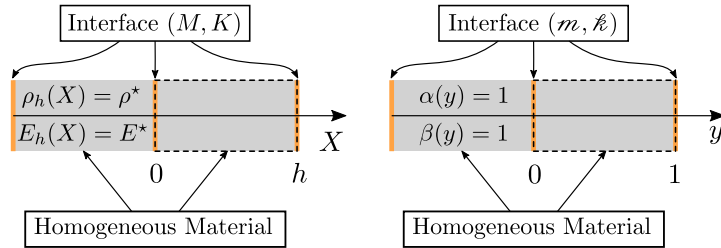


Figure 2: Geometry of the monolayer problem in the physical (left) and nondimensional (right) settings.

The Bloch-Floquet analysis (see Appendix B) gives the following dispersion relation

$$\cos(\kappa\delta) = \frac{1}{1 + \frac{m\mu^2}{4\ell}} \left[\left(1 - \frac{m\mu^2}{4\ell} \right) \cos(\mu) - \frac{1}{2} \left(\frac{\mu}{\ell} + m\mu \right) \sin(\mu) \right]. \quad (75)$$

The dispersion diagram classically displays band gaps as can be seen in Figure 3. We will now apply the high-frequency homogenisation technique to derive an analytical approximation to the higher branches of the diagram and to the associated wave fields.

In the case of a single eigenvalue, using (18), we find that \hat{u}_0 can be written as $\hat{u}_0 = A \cos(\mu_0 y) + B \sin(\mu_0 y)$ for some constants A and B , and, using Lemma 2.1, it is subject to the jump conditions

$$\begin{cases} \hat{u}_0(0^+) \mp \hat{u}_0(1^-) = \frac{1}{2\tilde{\kappa}} (\hat{u}'_0(0^+) \pm \hat{u}'_0(1^-)) \\ \hat{u}'_0(0^+) \mp \hat{u}'_0(1^-) = \frac{m\mu_0^2}{2} (\hat{u}_0(0^+) \pm \hat{u}_0(1^-)) \end{cases}, \quad (76)$$

where here and throughout the section, Notation 2.1 is being used. This leads to the relation

$$\mathcal{M}^{\text{mo}}(A, B)^T = (0, 0)^T, \quad (77)$$

where the 2×2 matrix $\mathcal{M}^{\text{mo}} = (\mathcal{M}_{ij}^{\text{mo}})$ is given by

$$\mathcal{M}^{\text{mo}} = \begin{pmatrix} 1 \mp \cos(\mu_0) \pm \frac{1}{2\tilde{\kappa}} \mu_0 \sin(\mu_0) & \mp \sin(\mu_0) - \frac{\mu_0}{2\tilde{\kappa}} (1 \pm \cos(\mu_0)) \\ \mp \mu_0 \sin(\mu_0) - \frac{m\mu_0^2}{2} (1 \pm \cos(\mu_0)) & -\mu_0 (1 \mp \cos(\mu_0)) \mp \frac{m\mu_0^2}{2} \sin(\mu_0) \end{pmatrix}.$$

The only way for non-trivial solutions to (77) to exist is for its determinant to be zero, which after some algebraic manipulations, leads to a dispersion relation of the form

$$\mathcal{D}^{\text{mo}}(\mu_0; m, \tilde{\kappa}) = 2(1 \mp \cos(\mu_0)) + \frac{m}{2\tilde{\kappa}} \mu_0^2 (1 \pm \cos(\mu_0)) \pm \mu_0 \sin(\mu_0) \left(m + \frac{1}{\tilde{\kappa}} \right) = 0, \quad (78)$$

where the fact that $\mu_0 \neq 0$ has been used (we are not here interested in the low frequency limit). In practice, when calculating μ_0 and reconstructing \hat{u}_0 , it can be useful to note that

$$\mathcal{M}_{22}^{\text{mo}} = \frac{\pm \sin(\mu_0)}{1 \pm \cos(\mu_0)} \mathcal{M}_{21}^{\text{mo}}, \quad \mathcal{M}_{12}^{\text{mo}} = \frac{1 \pm \cos(\mu_0)}{\mp \sin(\mu_0)} \mathcal{M}_{11}^{\text{mo}}, \quad \mathcal{M}_{11}^{\text{mo}} \mathcal{M}_{21}^{\text{mo}} = \mp \frac{\sin(\mu_0)}{2} \mathcal{D}^{\text{mo}}(\mu_0; m, \tilde{\kappa}), \quad (79)$$

so that μ_0 is either a zero of $\mathcal{M}_{11}^{\text{mo}}$ or $\mathcal{M}_{21}^{\text{mo}}$, and in the former (resp. latter) case, the top (resp. bottom) line of \mathcal{M}^{mo} is zero (it can be shown that $\sin(\mu_0) \neq 0$). The computed eigenvalues coincide with the edges of the Brillouin zone of the dispersion diagram of Figure 3. To obtain \hat{u}_0 , we set $A = 1$, so that $\hat{u}_0(0^+) = 1$, and compute B using the first (resp. second) line in (77) if $\mathcal{M}_{11}^{\text{mo}} \neq 0$ (resp. $\mathcal{M}_{21}^{\text{mo}} \neq 0$).

Because we are ultimately interested in the value of T in (48), we need to calculate $\langle \beta w_1 \rangle$ in (41), and hence v_1 on the interval $(0, 1)$. We do this using the fact that it satisfies the same second-order equation (18a) as \hat{u}_0 and can hence be written $v_1(y) = C \cos(\mu_0 y) + D \sin(\mu_0 y)$, for some constants C and D , which, using Remark 3.1, can be found by solving $\mathcal{M}^{\text{mo}}(C, D)^T = \mathbf{b}^{\text{mo}}$, where

$$\mathbf{b}^{\text{mo}} = \begin{pmatrix} \mp \hat{u}_0(1^-) \mp \frac{1}{2\tilde{\kappa}} \hat{u}'_0(1^-) \\ \mp \frac{m\mu_0^2}{2} \hat{u}_0(1^-) \pm \hat{u}'_0(1^-) \end{pmatrix}. \quad (80)$$

Since \mathcal{M}^{mo} is singular, (80) does not have a unique solution so we set $C = 1$ say and use the non-trivial line of the system to determine D . This works well since it can be shown that \mathbf{b}^{mo} is such that $\mathbf{b}_j^{\text{mo}} = 0$ whenever $\mathcal{M}_{j,1} = 0$.

Once v_1 is found, the resulting value of T is directly obtained using (41). Note that, in this simple case, no numerical integration is required and calculations can be performed analytically. The resulting second-order approximations $\mu \approx \mu_0 + \frac{T}{2\mu_0} (\tilde{\kappa}\delta)^2$ are superposed to the dispersion diagram in Figure 3 (left), and one can see that they approximate the branches well in the vicinity

of the edges of the Brillouin zone. One should also note that, as seen in Figure 4 (left), this approximation remains valid within the band gaps, where $\kappa\delta$ is complex and is such that $\text{Re}(\kappa\delta) = 0$. This is expected since in these cases, $(\kappa\delta)^2$ remain real. Having computed all the eigenvalues and eigenfunctions, it is now straightforward to compute T_d as per (62) and $\delta\gamma$ as per (66), where the pairs of eigenvalues are chosen naturally according to the dispersion diagram (first-second) and (third-fourth) in both the FFLW and FFFW cases. Hence we can evaluate the nearby eigenvalue approximation (74) derived in §5. It is displayed in Figure 3 (right), and as can clearly be seen, even if this approximation is only first-order in the vicinity of the edges of the Brillouin zone, its agreement with the dispersion diagram is much longer lived than that of the simple eigenvalue approximation. Similar observations are true within the band gaps as can be seen in Figure 4 (right)

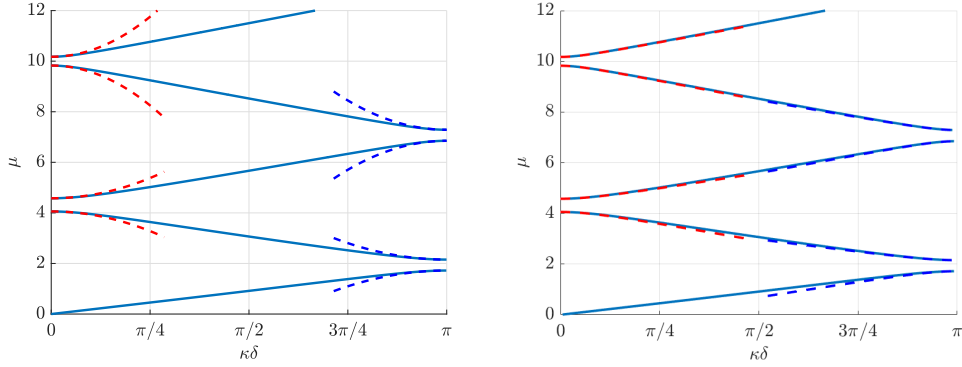


Figure 3: Dispersion diagram for the monolayer with $\ell = 1$ and $m = 0.5$. In red (resp. blue) dashed line are the periodic (resp. antiperiodic) second-order approximations (48) using the computed values of T (left) and nearby eigenvalue approximations (74) using the computed values of T_d and $\delta\gamma$ (right).

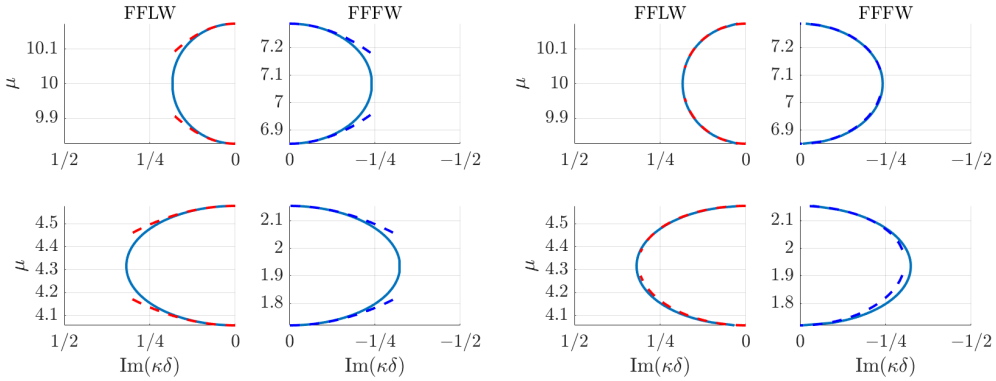


Figure 4: Imaginary part of $\kappa\delta$ in the band gaps of the monolayer dispersion diagram for $\ell = 1$ and $m = 0.5$. In red (resp. blue) dashed lines are the periodic (resp. antiperiodic) second-order approximations (48) using the computed values of T (left) and nearby eigenvalue approximations (74) using the computed values of T_d and $\delta\gamma$ (right).

We will now investigate the accuracy of the zeroth-order field approximation obtained in

the simple eigenvalue case. Using the Bloch-Floquet analysis (see [Appendix B](#)), we can have access to the exact standing wave field $u_\delta(x) = u_\delta(\delta y)$, and, to be compatible with the asymptotic expansion (12), we normalise it such that $u_\delta(0^+) = u_0(0, 0^+)$. Note that because of (10) and (50), the difference between the exact and approximated field can be written as

$$u_\delta(x) - u_0\left(x, \frac{x}{\delta}\right) = u_\delta(\delta y) - u_0(\delta y, y) = \begin{cases} e^{i\kappa\delta y}(u_\delta(\delta y) - \hat{u}_0(y)) & \text{(FFLW)}, \\ e^{i\kappa\delta y}(u_\delta(\delta y) - e^{-i\pi y}\hat{u}_0(y)) & \text{(FFFW)}. \end{cases} \quad (81)$$

To illustrate the validity of our approximation, we hence compare $u_\delta(\delta y)$ and $\hat{u}_0(y)$ for various values of $\kappa\delta$ in Figure 5, showing, as expected, that as $\kappa\delta$ gets smaller the zeroth-order field is a good approximation to the exact field.

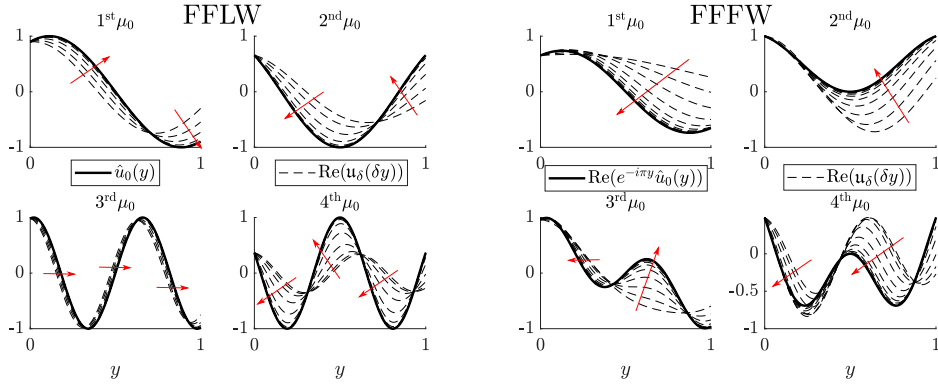


Figure 5: Illustration of the convergence of the method by comparing \hat{u}_0 and $u_\delta(\delta y)$ in the FFLW (left) and the FFFW (right) cases. We plotted u_δ for 20 values of $\kappa\delta$ equidistributed in the log scale between 10^{-5} and 1. The red arrows indicate how $u_\delta(\delta y)$ is changing as $\kappa\delta \rightarrow 0$.

A similar investigation can be carried out for the nearby eigenvalue approximation of the field. As can be seen in Figure 6, the approximation is good for a value of $\kappa\delta = 0.5$ that is not particularly small, and for which the agreement of the simple eigenvalue zeroth-order field is poor.

In Figure 7, we plot the error between the exact field and the *homogenised* fields obtained using both the simple and nearby eigenvalue approximations. Due to the periodicity properties of u_δ and \hat{u}_0 and (81), the error is relatively easy to compute in the simple eigenvalue case and is defined as follows:

$$\text{(FFLW): } \mathcal{E}_{\text{simple}}^{\text{FFLW}} = \max_{\mathbb{R}} |u_\delta(\delta y) - u_0(\delta y, y)| = \max_{(0,1)} |u_\delta(\delta y) - \hat{u}_0(y)|, \quad (82)$$

$$\text{(FFFW): } \mathcal{E}_{\text{simple}}^{\text{FFFW}} = \max_{\mathbb{R}} |u_\delta(\delta y) - u_0(\delta y, y)| = \max_{(0,1)} |u_\delta(\delta y) - e^{-i\pi y}\hat{u}_0(y)|. \quad (83)$$

In the nearby eigenvalue approximation, using (51), (72) and (63), the errors can be written as

$$\text{(FFLW): } \mathcal{E}_{\text{nearby}}^{\text{FFLW}} = \max_{(0,1)} \left| u_\delta(\delta y) - \left(\frac{-\langle \beta w_0 \rangle}{(mB_1^2 + C_1)} \frac{i\tilde{\kappa}\delta}{\delta\mu_1^2} \hat{u}_0^{(1)}(y) + \hat{u}_0^{(2)}(y) \right) \right|, \quad (84)$$

$$\text{(FFFW): } \mathcal{E}_{\text{nearby}}^{\text{FFFW}} = \max_{(0,1)} \left| u_\delta(\delta y) - e^{-i\pi y} \left(\frac{-\langle \beta w_0 \rangle}{(mB_1^2 + C_1)} \frac{i\tilde{\kappa}\delta}{\delta\mu_1^2} \hat{u}_0^{(1)}(y) + \hat{u}_0^{(2)}(y) \right) \right|. \quad (85)$$

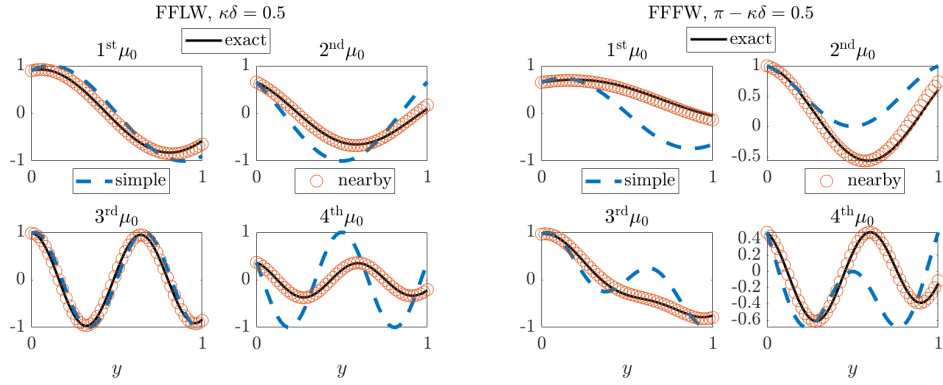


Figure 6: Superposition of real parts of the exact (u_δ), simple eigenvalue zeroth-order (\hat{u}_0) and nearby eigenvalue approximation normalized wave fields in the FFLW (left) and FFFW (right) for $\kappa\delta = 0.5$

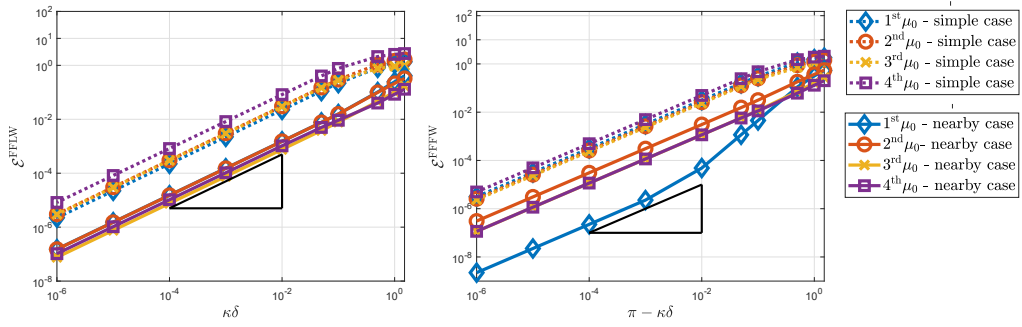


Figure 7: Loglog plot of the error between the exact (Bloch Floquet) and the homogenised fields for various values of $\kappa\delta$ with $\ell = 1$ and $m = 0.5$. (Left) FFLW. (Right) FFFW. The slope depicted by a black triangle denotes a $O(\kappa\delta)$. Dotted (resp. plain) lines correspond to the simple (resp. nearby) eigenvalue approximations.

One can see that we recover the expected behaviour $u_\delta(\delta y) = u_0(\delta y, y) + O(\tilde{\kappa}\delta)$, but that the nearby eigenvalue approximation performs much better for the whole range of values of $\tilde{\kappa}\delta$ used in Figure 7.

We now endeavour to study how the eigenvalues μ_0 depend on m and $\tilde{\kappa}$. In order to visualise this we display a heat map of the first and second FFLW (periodic) $\mu_0(m, \tilde{\kappa})$ in Figure 8. One can clearly see two distinct regions, on the left and on the right of the curve $\tilde{\kappa} = 1/m$. On each side of these curves, the eigenvalue depend solely on one of the two parameters ($m, \tilde{\kappa}$), which correspond to either the top or the bottom line of \mathcal{M}^{mo} being zero. On the curve $\tilde{\kappa} = 1/m$, both lines of \mathcal{M}^{mo} are zero, and hence, the eigenvalue μ_0 is a double eigenvalue.

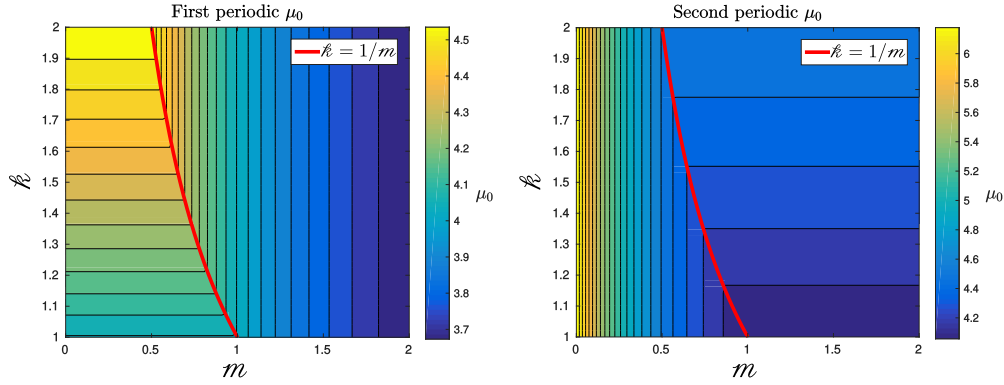


Figure 8: Filled contour plot of the first (left) and second (right) periodic eigenvalues μ_0 as m and $\tilde{\kappa}$ vary. The thick red line represents the locus of double eigenvalues, while the thin black lines are isolines of μ_0 .

The other eigenvalues in the the FFLW (periodic) and FFFW (antiperiodic) case have very similar heatmaps, in particular they are all double eigenvalues when $\tilde{\kappa} = 1/m$, as displayed on the dispersion diagram in Figure 9 (left).

In the case of a double eigenvalue, we have to follow the procedure of §4 by representing u_0 as in (51). We hence need to find two independent solutions $\hat{u}_0^{(1,2)}$ of (18), which can both be written $\hat{u}_0^{(1,2)}(y) = A^{(1,2)} \cos(\mu_0 y) + B^{(1,2)} \sin(\mu_0 y)$. Because of the dimension of the system, any two independent vectors $(A^{(1)}, B^{(1)})^T$ and $(A^{(2)}, B^{(2)})^T$ would work, and we can hence choose $(A^{(1)}, B^{(1)})^T = (1, 0)^T$ and $(A^{(2)}, B^{(2)})^T = (0, 1)^T$. As seen in §4, the two functions $\mathcal{U}_0^{(1,2)}(x)$ appearing in (51) satisfy the first-order ODE system (59), where in our case we have

$$B_1 = \langle \hat{u}_0^{(1)} \rangle = \frac{1 \pm \cos(\mu_0)}{2}, \quad B_2 = \langle \hat{u}_0^{(2)} \rangle = \frac{\pm \sin(\mu_0)}{2}, \quad C_1 = \langle \alpha(\hat{u}_0^{(1)})^2 \rangle = \frac{\mu_0 + \sin(\mu_0) \cos(\mu_0)}{2\mu_0},$$

$$D = \langle \alpha \hat{u}_0^{(1)} \hat{u}_0^{(2)} \rangle = \frac{\sin^2(\mu_0)}{2\mu_0}, \quad \langle \beta w_0 \rangle = \mu_0, \quad C_2 = \langle \alpha(\hat{u}_0^{(2)})^2 \rangle = \frac{\mu_0 - \sin(\mu_0) \cos(\mu_0)}{2\mu_0}.$$

Using these, one can easily compute the associated eigenvalues $\lambda_{1,2}$ and eigenvectors $\mathcal{U}_{\lambda_{1,2}}$ via (60) and (61). Note that in this case, one can show that

$$mB_1B_2 + D = 0 \quad \text{and} \quad mB_1^2 + C_1 = mB_2^2 + C_2,$$

so that the eigenvalues $\lambda_{1,2}$ and eigenvectors $\mathbf{U}_{\lambda_{1,2}}$ of the matrix of the ODE system are simply

$$\lambda_j = i(-1)^j(mB_1^2 + C_1) \quad \text{and} \quad \mathbf{U}_{\lambda_j} = (-i(-1)^j, 1)^T,$$

and $T_d = \mu_0/(mB_1^2 + C_1)$. We can hence superpose the resulting linear approximation (65) onto the dispersion diagram, revealing an excellent fit, as can be seen in Figure 9 (right). It is quite remarkable that in this case, every eigenvalues μ_0 correspond to Dirac points. In fact this can be understood by considering a homogeneous material with only one spring-mass interface. Upon sending a wave onto this interface, one can naturally derive a coefficient of reflection $\text{Ref}(\mu)$ and a coefficient of transmission $\text{Trans}(\mu)$. It turns out that

$$\text{Ref}(\mu) = \frac{-i\mu\left(\frac{1}{\mathcal{K}} - m\right)}{2\left(1 - \frac{m\mu^2}{4\mathcal{K}}\right) - i\mu\left(\frac{1}{\mathcal{K}} + m\right)} \quad \text{and} \quad \text{Trans}(\mu) = \frac{2\left(1 + \frac{m\mu^2}{4\mathcal{K}}\right)}{2\left(1 - \frac{m\mu^2}{4\mathcal{K}}\right) - i\mu\left(\frac{1}{\mathcal{K}} + m\right)},$$

and therefore the reflection coefficient is zero if and only if the condition $\mathcal{K} = 1/m$ is satisfied. Hence, in the periodic medium considered, no internal reflection can be present, no destructive/constructive interference can take place and no band gaps occur.

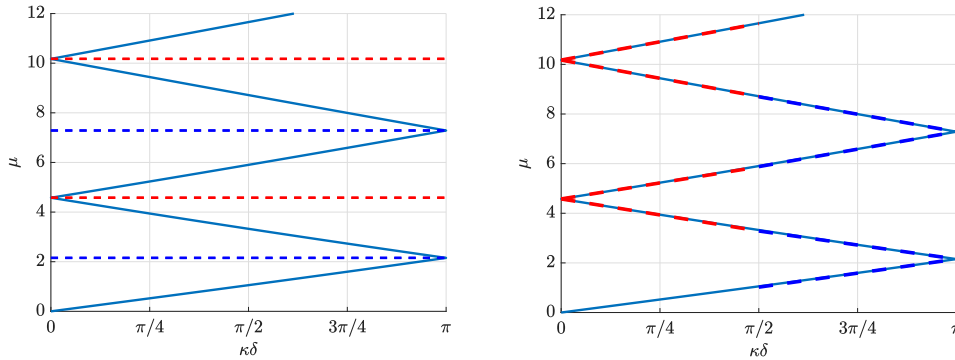


Figure 9: Dispersion diagram for the monolayer with $\mathcal{K} = 2$ and $m = 0.5$ corresponding to double eigenvalues. (Left) In red (resp. blue) dashed lines are the periodic (resp. antiperiodic) eigenvalues μ_0 calculated by finding the roots of (78). (Right) In red (resp. blue) dashed lines are the periodic (resp. antiperiodic) resulting first-order approximations (65).

6.2. Bilayer

We now consider the case of a bilayer material characterised by the phase fraction $r \in (0, 1)$, and hence provide the imperfect interface extension to the example given in [6]. The unit cell is made up of two homogeneous materials. The first one has a length rh , density ρ_1 and Young's modulus E_1 , while the second has length $(1-r)h$, density ρ_2 and Young's Modulus E_2 . The two respective wave speeds are $c_1 = \sqrt{E_1/\rho_1}$ and $c_2 = \sqrt{E_2/\rho_2}$. The important non dimensional functions α and β are hence defined by

$$\alpha(y) = \begin{cases} \alpha^{(1)} = \rho_1/\rho^* & \text{for } y \in (0, r), \\ \alpha^{(2)} = \rho_2/\rho^* & \text{for } y \in (r, 1), \end{cases} \quad \text{and} \quad \beta(y) = \begin{cases} \beta^{(1)} = E_1/E^* & \text{for } y \in (0, r), \\ \beta^{(2)} = E_2/E^* & \text{for } y \in (r, 1), \end{cases} \quad (86)$$

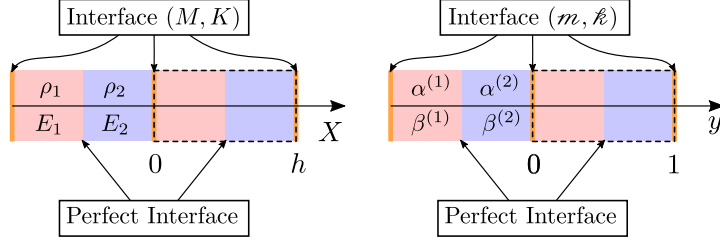


Figure 10: Geometry of the bilayer problem (left) and non-dimensional (right) settings.

where $\rho^* = r\rho_1 + (1-r)\rho_2$ and $E^* = (r/E_1 + (1-r)/E_2)^{-1}$. The interface at $y = r$ is assumed perfect, and the geometry of this physical problem is summarised in Figure 10.

The classic Bloch-Floquet analysis will, in this case, give the following dispersion relation

$$\cos(\kappa\delta) = \frac{1}{1 + \frac{m\mu^2}{4\ell}} \left[\left(1 - \frac{m\mu^2}{4\ell} \right) \left(C_1 C_2 - \frac{1}{2} \left(\frac{Z_1}{Z_2} + \frac{Z_2}{Z_1} \right) S_1 S_2 \right) - \frac{m\mu}{2} \left(\frac{S_1 C_2 Z^*}{Z_1} + \frac{S_2 C_1 Z^*}{Z_2} \right) - \frac{\mu}{2\ell} \left(\frac{Z_1 S_1 C_2}{Z^*} + \frac{Z_2 S_2 C_1}{Z^*} \right) \right], \quad (87)$$

where $Z^* = \rho^* c^*$, and $C_i = \cos(\mu H_i)$, $S_i = \sin(\mu H_i)$, $H_1 = rc^*/c_1$, $H_2 = (1-r)c^*/c_2$ and, naturally, $c^* = \sqrt{E^*/\rho^*}$. As per the monolayer case, the dispersion diagram displays band gaps as can be seen in Figure 11. We will now apply the high-frequency homogenisation technique to derive an analytical approximation to the higher branches of the diagram and to the associated wave fields.

Using (18a) and (21), we find that \hat{u}_0 should satisfy

$$\begin{cases} \hat{u}_0'' + (\Omega^{(1)})^2 \hat{u}_0 = 0 & \text{on } (0, r), \\ \hat{u}_0'' + (\Omega^{(2)})^2 \hat{u}_0 = 0 & \text{on } (r, 1), \end{cases} \quad \text{so that} \quad \begin{cases} \hat{u}_0(y) = A^{(1)} \cos(\Omega^{(1)}y) + B^{(1)} \sin(\Omega^{(1)}y) & \text{on } (0, r), \\ \hat{u}_0(y) = A^{(2)} \cos(\Omega^{(2)}y) + B^{(2)} \sin(\Omega^{(2)}y) & \text{on } (r, 1), \end{cases} \quad (88)$$

where $A^{(1,2)}$ and $B^{(1,2)}$ are some constants to be determined, and $\Omega^{(1,2)} = \mu_0 \sqrt{\frac{\alpha^{(1,2)}}{\beta^{(1,2)}}} = \mu_0 \frac{c^*}{c_{1,2}}$. The interface at $y = r$ is assumed perfect, and hence, \hat{u}_0 is also subject to the interface conditions

$$\begin{cases} \hat{u}_0(r^-) = \hat{u}_0(r^+), \\ \beta^{(1)} \hat{u}_0'(r^-) = \beta^{(2)} \hat{u}_0'(r^+), \end{cases} \quad \text{and} \quad \begin{cases} \hat{u}_0(0^+) \mp \hat{u}_0(1^-) = \frac{1}{2\ell} (\beta^{(1)} \hat{u}_0'(0^+) \pm \beta^{(2)} \hat{u}_0'(1^-)), \\ \beta^{(1)} \hat{u}_0'(0^+) \mp \beta^{(2)} \hat{u}_0'(1^-) = -\frac{m\mu_0^2}{2} (\hat{u}_0(0^+) \pm \hat{u}_0(1^-)), \end{cases}$$

where here and throughout this section, Notation 2.1 is being used. This results in a system of the form

$$\mathcal{M}^{\text{bi}}(A^{(1)}, B^{(1)}, A^{(2)}, B^{(2)})^T = (0, 0, 0, 0)^T, \quad (89)$$

where the 4×4 matrix \mathcal{M}^{bi} is given by

$$\mathcal{M}^{\text{bi}} = \begin{pmatrix} 1 & -\frac{\beta^{(1)}\Omega^{(1)}}{2\ell} & \mp \cos(\Omega^{(2)}) \pm \frac{\beta^{(2)}\Omega^{(2)}\sin(\Omega^{(2)})}{2\ell} & \mp \sin(\Omega^{(2)}) \mp \frac{\beta^{(2)}\Omega^{(2)}\cos(\Omega^{(2)})}{2\ell} \\ -\frac{m\mu_0^2}{2} & -\beta^{(1)}\Omega^{(1)} & \mp \beta^{(2)}\Omega^{(2)}\sin(\Omega^{(2)}) \mp \frac{m\mu_0^2}{2}\cos(\Omega^{(2)}) & \pm \beta^{(2)}\Omega^{(2)}\cos(\Omega^{(2)}) \mp \frac{m\mu_0^2}{2}\sin(\Omega^{(2)}) \\ -\cos(\Omega^{(1)}r) & -\sin(\Omega^{(1)}r) & \cos(\Omega^{(2)}r) & \sin(\Omega^{(2)}r) \\ \beta^{(1)}\Omega^{(1)}\sin(\Omega^{(1)}r) & -\beta^{(1)}\Omega^{(1)}\cos(\Omega^{(1)}r) & -\beta^{(2)}\Omega^{(2)}\sin(\Omega^{(2)}r) & \beta^{(2)}\Omega^{(2)}\cos(\Omega^{(2)}r) \end{pmatrix}. \quad (24)$$

The equation (89) can only have non-trivial solutions if $\det(\mathcal{M}^{\text{bi}}) = 0$, which gives a relation of the form

$$\mathcal{D}^{\text{bi}}(\mu_0; m, \kappa, \beta^{(1)}, \beta^{(2)}, \Omega^{(1)}, \Omega^{(2)}, r) = 0, \quad (90)$$

the roots of which correspond to the eigenvalues μ_0 . The numerically computed eigenvalues coincide with the edges of the Brillouin zone on the dispersion diagram in Figure 11. To obtain \hat{u}_0 , we find a vector in $\ker(\mathcal{M}^{\text{bi}})$ using the `null` function in Matlab, and use it as the coefficients $(A^{(1)}, B^{(1)}, A^{(2)}, B^{(2)})$.

We now need to find v_1 to obtain a second-order approximation. Since it is solution to the same equation (18a), we can write

$$v_1(y) = \begin{cases} C^{(1)} \cos(\Omega^{(1)}y) + D^{(1)} \sin(\Omega^{(1)}y) & \text{on } (0, r), \\ C^{(2)} \cos(\Omega^{(2)}y) + D^{(2)} \sin(\Omega^{(2)}y) & \text{on } (r, 1). \end{cases} \quad (91)$$

Using Remark 3.1 for the conditions at the unit cell interfaces, and remembering that, according to Remark 3.2, both v_1 and $\beta v_1'$ should be continuous at $y = r$, one obtains a system of the form $\mathcal{M}^{\text{bi}}(C^{(1)}, D^{(1)}, C^{(2)}, D^{(2)})^T = \mathbf{b}^{\text{bi}}$, where

$$\mathbf{b}^{\text{bi}} = \left(\mp \hat{u}_0(1^-) \mp \frac{1}{2\kappa} \beta^{(2)} \hat{u}'_0(1^-), \mp \frac{m\mu_0^2}{2} \hat{u}_0(1^-) \pm \beta^{(2)} \hat{u}'_0(1^-), 0, 0 \right)^T.$$

Because the matrix \mathcal{M}^{bi} is singular, we compute $(C^{(1)}, D^{(1)}, C^{(2)}, D^{(2)})^T$ via the Moore-Penrose Pseudo-inverse [29]. Once v_1 is found, the resulting value of T is directly obtained using (41). The resulting approximations $\mu \approx \mu_0 + \frac{T}{2\mu_0} (\tilde{\kappa}\delta)^2$ are superposed to the Bloch-Floquet diagram in Figure 11 (left), and one can see that they approximate the branches well in the vicinity of the edges of the band gaps of the dispersion diagram. It is apparent from Figure 11 that the highest antiperiodic eigenvalue displayed seems to be a double eigenvalue (in fact we will see further that it is not exactly a double eigenvalue), and that the approximation is particularly short-lived in this neighbourhood. Having computed all the eigenvalues and eigenfunctions, we can once again evaluate the nearby eigenvalue approximation (74). It is displayed in Figure 11 (right), and as can clearly be seen, its agreement with the dispersion diagram is much longer-lived than of the simple eigenvalue approximation, even more so for the near-double eigenvalue.

Using the Bloch-Floquet analysis, in a very similar way to the monolayer case, we can have access to the exact standing wave field $u_\delta(x) = u_\delta(\delta y)$, and we normalise it such that $u_\delta(0^+) = u_0(0, 0^+)$. As per the monolayer case, and because of (81), we illustrate the convergence of the simple eigenvalue method by comparing $u_\delta(\delta y)$ and $\hat{u}_0(y)$ for various values of $\kappa\delta$ in Figure 12.

A similar investigation can be carried out for the nearby eigenvalue approximation. As can be seen in Figure 13, the approximation is good even for a value of $\tilde{\kappa}\delta = 0.5$ that is not particularly small, and for which the agreement of the simple eigenvalue zeroth-order field is poor.

In Figure 14, we plot the error between the exact field and the *homogenised* fields obtained using both the simple and nearby eigenvalue approximations. The errors can be expressed as in (82)–(85). Again, one can see that we recover the expected behaviour $u_\delta(\delta y) = u_0(\delta y, y) + O(\tilde{\kappa}\delta)$, but that the nearby eigenvalue approximation performs better for the whole range of values of $\tilde{\kappa}\delta$ used in Figure 14.

As for the monolayer example displayed in Figure 9, it is possible to find physical parameters such that all the eigenvalues become simultaneously double eigenvalues (Dirac points). In order to do so one needs to ensure that $\kappa = 1/m$, and that $\rho_1 c_1 = \rho_2 c_2$. The first condition imposes

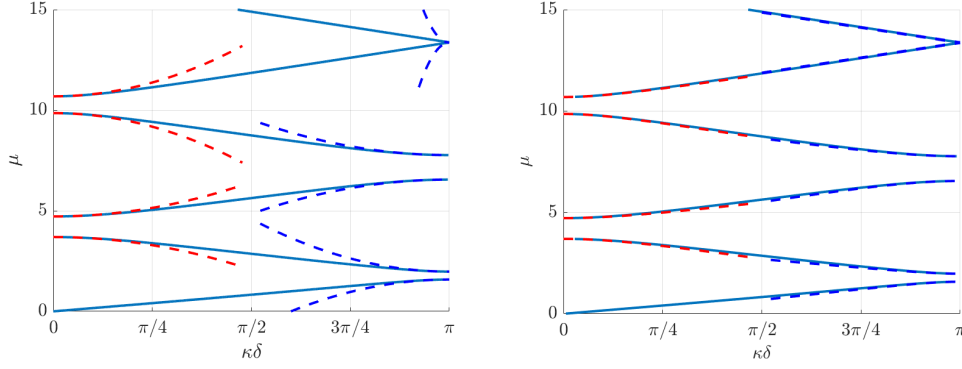


Figure 11: Non-dimensional dispersion diagram for the bilayer with $\rho_1 = 1200 \text{ kg.m}^{-3}$, $\rho_2 = 1800 \text{ kg.m}^{-3}$, $c_1 = 2800 \text{ m.s}^{-1}$, $c_2 = 3500 \text{ m.s}^{-1}$, $E_1 = \rho_1 c_1^2$, $E_2 = \rho_2 c_2^2$, $M = 2 \times 10^4 \text{ kg.m}^2$, $K = 2.45 \times 10^9 \text{ Pa.m}^{-1}$, $r = 0.202$ and $h = 10 \text{ m}$, corresponding to $\ell \approx 1.41$ and $m \approx 1.19$, $\alpha^{(1)} \approx 0.71$, $\alpha^{(2)} \approx 1.071$, $\beta^{(1)} \approx 0.54$ and $\beta^{(2)} \approx 1.27$. The red (resp. blue) dashed lines are the periodic (resp. antiperiodic) second-order approximations (48) using the computed values of T (left) and nearby eigenvalue approximations (74) using the computed values of T_d and $\delta\gamma$ (right).

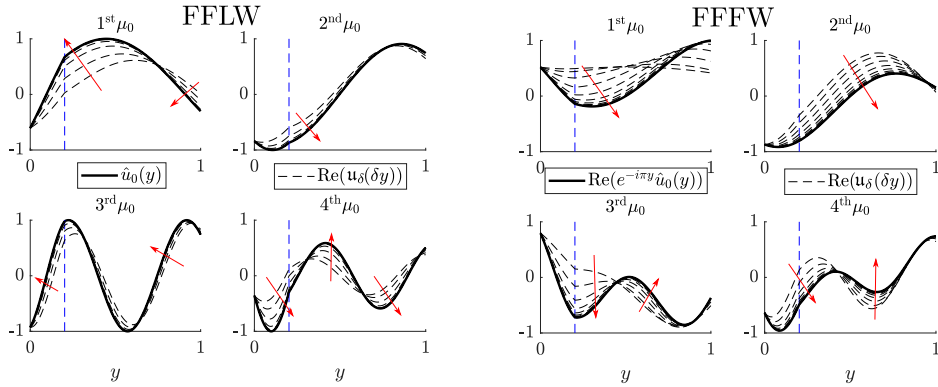


Figure 12: Illustration of the convergence of the method by comparing \hat{u}_0 and $u_\delta(\delta y)$ in the FFLW (left) and the FFFW (right) cases. We plotted u_δ for 20 values of $\bar{\kappa}\delta$ equidistributed in the log scale between 10^{-5} and 1. The red arrows indicate how $u_\delta(\delta y)$ is changing as $\bar{\kappa}\delta \rightarrow 0$, while the vertical dashed blue line indicates the position of the perfect interface between the two homogeneous materials.

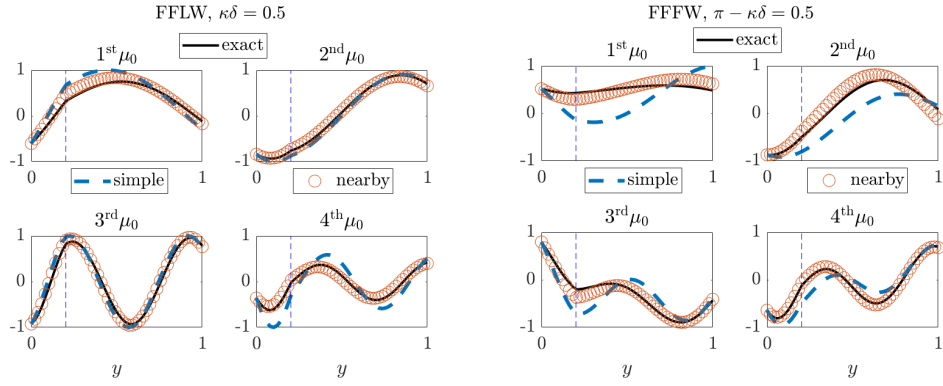


Figure 13: Superposition of real parts of the exact (u_δ), simple eigenvalue zeroth-order (\hat{u}_0) and nearby eigenvalue approximation normalised wave fields in the FFLW (left) and FFFW (right) for $\bar{\kappa}\delta = 0.5$ and for the same parameters used in Figure 11.

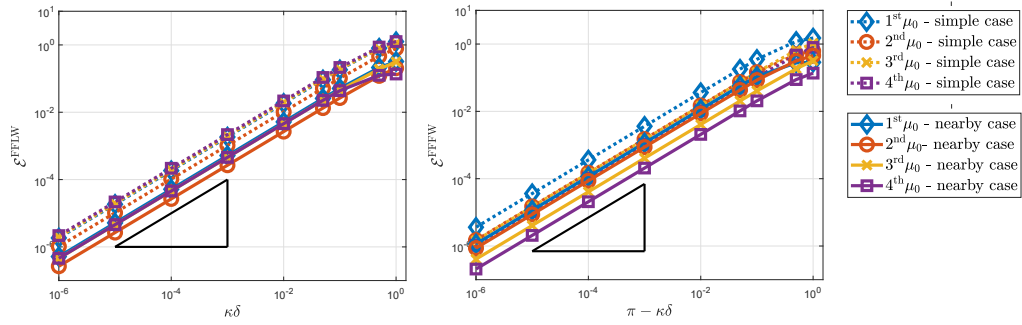


Figure 14: Loglog plot of the error between the exact (Bloch Floquet) and the homogenised fields for various values of $\kappa\delta$ and for the same parameters used in Figure 11. (Left) FFLW. (Right) FFFW. The slope depicted by a black triangle denotes a $O(\bar{\kappa}\delta)$. Dotted (resp. plain) lines correspond to the simple (resp. nearby) eigenvalue approximation.

that the reflection coefficient due to the imperfect interface is zero, and the second imposes that the two homogeneous materials are “impedance matched” so that no reflection occurs from their perfect interface either.

However, for the bilayer, it appears that certain parameters lead to only two of the eigenvalues merging into a double eigenvalue, as appears to be the case in Figure 11. In order to visualise this phenomena, one could look at the evolution of the eigenvalues μ_0 for fixed physical parameter, but for varying r within $(0, 1)$. The results are displayed in Figure 15, and it seems that double eigenvalues or near-double eigenvalues may occur for some specific values of r , though, in this case, all the eigenvalues do not become double simultaneously. In fact, as illustrated in Figure 15, if one zooms on the areas of the graphs where eigenvalues seem to coincide, it appears that the curves do not actually touch each other. We will call these points *almost-Dirac points*. As highlighted above, the nearby eigenvalue approximation to the dispersion diagram is excellent for such almost-Dirac points, while the simple eigenvalue method leads to a very short-lived approximation, see Figure 11.

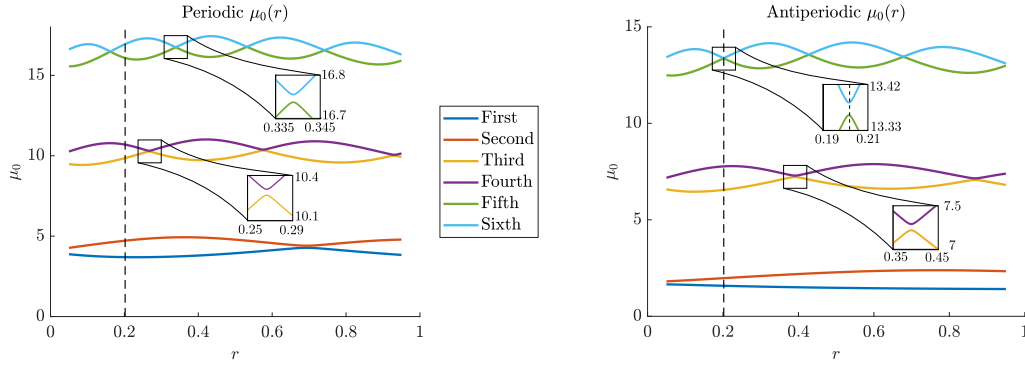


Figure 15: Evolution of the first six FFLW (left) and FFFW (right) eigenvalues μ_0 for the exact same parameters as those used in Figure 11, but for $r \in (0.05, 0.95)$. A vertical dashed line represents the value of r used in Figure 11. Zoom boxes are provided to show that near the almost-Dirac points, the eigenvalues remain simple.

To explore the parameter space further, we will keep the values of r , $\alpha^{(1,2)}$ and $\beta^{(1,2)}$ used in Figure 11 and study the variation of the fifth and sixth antiperiodic eigenvalues μ_0 that correspond to an almost-Dirac point according to Figure 15. As can be seen in Figure 16, in this case, we observe a similar behaviour as that of Figure 8, where two distinct regions seem to be separated by a smooth curve, on which the values of m and ℓ chosen in Figure 11 (represented by a black star) seem to lie.

All in all, it seems to be the case, that for a given integer j , the j^{th} eigenvalue is double on some manifold given by $\mathfrak{F}_j(\rho_1, \rho_2, E_1, E_2, M, K, r) = 0$ for some function \mathfrak{F}_j , though finding an analytical expression for \mathfrak{F}_j is beyond the scope of the present work.

7. Conclusion

In this work, we have extended the technique of high-frequency homogenisation to one-dimensional periodic media with linear imperfect interfaces of the spring-mass type. The extension was not direct, and many of the proofs for the classic case needed to be extended in order to deal with the extra technical difficulties arising from imperfect interface. We have also described

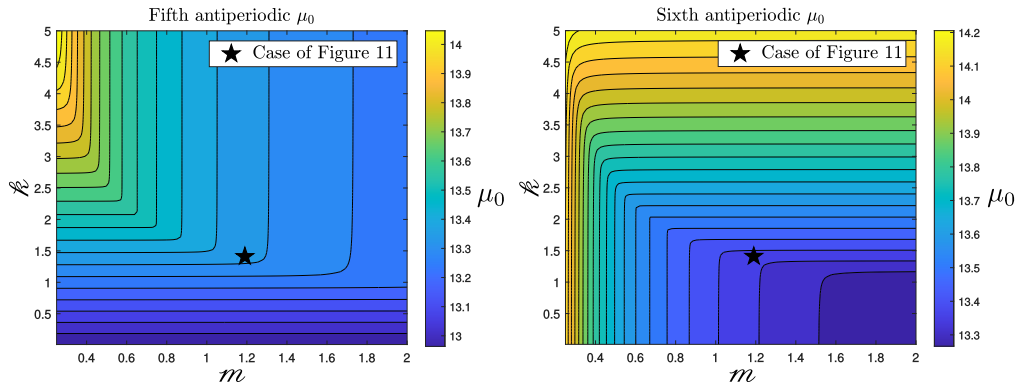


Figure 16: Filled Contour Plot of the variations of the fifth (left) and sixth (right) antiperiodic eigenvalues in the bilayer case for the same values of r , $\alpha^{(1,2)}$ and $\beta^{(1,2)}$ used in Figure 11. The black star corresponds to the values of m and ℓ used in Figure 11.

how the technique should be modified in the specific case of Dirac points within the dispersion diagram, and also proposed a uniform approximation taking into consideration competing nearby eigenvalues.

We have illustrated the validity of our theoretical development with the two examples of monolayered and bilayered materials. In the case of the monolayered material, we quantified the error between the exact and the homogenised fields, and we found a simple condition on the nondimensional stiffness and mass values ℓ and m for all the points at the edges of the Brillouin zone to become Dirac points. Similar conditions were given in the bilayered case. Moreover, in the bilayered case, almost-Dirac points have been identified while exploring the parameter space (much larger than that of the monolayered material). For both examples considered, we found that the nearby eigenvalue approximation led to a much-longer-lived approximation to both the dispersion diagram and the wave fields. This formulation is also convenient because it does not breakdown when two eigenvalues merge, unlike the simple eigenvalue approximation. As mentioned previously, one of the advantages of high-frequency homogenisation is that it works even when the dispersion diagrams cannot be obtained analytically or are computationally intricate to obtain. In such cases, this high-frequency homogenisation approach may, for example, provide a way of back-engineering the values of m and ℓ describing imperfect interface, or pick specific material properties and contact in order to ensure the presence of Dirac points, which are known to display very interesting physical properties.

In the future, we hope to be able to push the asymptotics presented in this paper to higher order, i.e. to propose first- and maybe second-order corrections to the leading-order wave fields exhibited in the present work.

Appendix A. On the self-adjointness of (18)

The system (18) is the eigenvalue problem that can be formulated as follows. Find λ such that $\mathcal{L}[f] = \lambda f$ with $\llbracket f \rrbracket = \frac{1}{\ell} \langle\langle \beta \frac{df}{dy} \rangle\rangle$ (1st jump) and $\llbracket \beta \frac{df}{dy} \rrbracket = -m\lambda \langle\langle f \rangle\rangle$ (2nd jump), for some function f that is periodic (FFLW) or antiperiodic (FFFW). It is somewhat inconvenient for λ to appear in the second jump, so we rewrite it as $\llbracket \beta \frac{df}{dy} \rrbracket = -m \langle\langle \mathcal{L}[f] \rangle\rangle$ (2nd jump). We will now show that the operator \mathcal{L} , together with the jump and periodicity conditions is both symmetric

and non-negative for the inner product (19), that is $\langle \mathcal{L}[f], g \rangle = \langle f, \mathcal{L}[g] \rangle$ and $\langle \mathcal{L}[f], f \rangle \geq 0$ for any functions f and g satisfying both jump conditions and both periodic (FFLW) or antiperiodic (FFFW). To prove symmetry, we will show that the quantity $\text{Sym}(f, g) = \langle \mathcal{L}[f], g \rangle - \langle f, \mathcal{L}[g] \rangle$ is zero. First by definition of the inner product (19) we have

$$\begin{aligned} \text{Sym}(f, g) &= \langle \alpha \mathcal{L}[f] \bar{g} \rangle + m \langle \mathcal{L}[f] \rangle \langle \bar{g} \rangle - \langle \alpha f \overline{\mathcal{L}[g]} \rangle - m \langle f \rangle \langle \overline{\mathcal{L}[g]} \rangle \\ &\stackrel{\text{2nd jump}}{=} \left\langle f \frac{d}{dy} \left(\beta \frac{d\bar{g}}{dy} \right) - \frac{d}{dy} \left(\beta \frac{df}{dy} \right) \bar{g} \right\rangle + \langle f \rangle \left[\left\langle \beta \frac{d\bar{g}}{dy} \right\rangle - \left[\left\langle \beta \frac{df}{dy} \right\rangle \right] \langle \bar{g} \rangle \right]. \end{aligned} \quad (\text{A.1})$$

Now, using the fact that $f \frac{d}{dy} \left(\beta \frac{d\bar{g}}{dy} \right) - \frac{d}{dy} \left(\beta \frac{df}{dy} \right) \bar{g} = \frac{d}{dy} \left(f \beta \frac{d\bar{g}}{dy} - \beta \frac{df}{dy} \bar{g} \right)$, (A.1) becomes

$$\begin{aligned} \text{Sym}(f, g) &= \left\langle \frac{d}{dy} \left(f \beta \frac{d\bar{g}}{dy} - \beta \frac{df}{dy} \bar{g} \right) \right\rangle + \langle f \rangle \left[\left\langle \beta \frac{d\bar{g}}{dy} \right\rangle - \left[\left\langle \beta \frac{df}{dy} \right\rangle \right] \langle \bar{g} \rangle \right] \\ &\stackrel{\text{Lemma 2.3}}{=} - \left[\left\langle f \beta \frac{d\bar{g}}{dy} - \beta \frac{df}{dy} \bar{g} \right\rangle + \langle f \rangle \left[\left\langle \beta \frac{d\bar{g}}{dy} \right\rangle - \left[\left\langle \beta \frac{df}{dy} \right\rangle \right] \langle \bar{g} \rangle \right] \right] \\ &\stackrel{\text{Lemma 2.2}}{=} \left[\left\langle \beta \frac{df}{dy} \right\rangle \right] \langle \bar{g} \rangle - \left[\left\langle \beta \frac{d\bar{g}}{dy} \right\rangle \right] \langle f \rangle \stackrel{\text{1st jump}}{=} \mathcal{K}[\mathbb{I}f] \langle \bar{g} \rangle - \mathcal{K}[\mathbb{I}f] \langle \bar{g} \rangle = 0, \end{aligned}$$

and hence the problem is symmetric. Now, by definition of the inner product (19), we have

$$\langle \mathcal{L}[f], f \rangle = \langle \alpha \mathcal{L}[f] \bar{f} \rangle + m \langle \mathcal{L}[f] \rangle \langle \bar{f} \rangle \stackrel{\text{2nd jump}}{=} \left\langle \frac{d}{dy} \left(\beta \frac{df}{dy} \right) \bar{f} \right\rangle - \left[\left\langle \beta \frac{df}{dy} \right\rangle \right] \langle \bar{f} \rangle. \quad (\text{A.2})$$

Now, using the fact that $\frac{d}{dy} \left(\beta \frac{df}{dy} \right) \bar{f} = \frac{d}{dy} \left(\beta \frac{df}{dy} \bar{f} \right) - \beta \left| \frac{df}{dy} \right|^2$, (A.2) becomes

$$\begin{aligned} \langle \mathcal{L}[f], f \rangle &= \left\langle \beta \left| \frac{df}{dy} \right|^2 \right\rangle - \left\langle \frac{d}{dy} \left(\beta \frac{df}{dy} \bar{f} \right) \right\rangle - \left[\left\langle \beta \frac{df}{dy} \right\rangle \right] \langle \bar{f} \rangle \\ &\stackrel{\text{Lemma 2.3}}{=} \left\langle \beta \left| \frac{df}{dy} \right|^2 \right\rangle + \left[\left\langle \beta \frac{df}{dy} \bar{f} \right\rangle - \left[\left\langle \beta \frac{df}{dy} \right\rangle \right] \langle \bar{f} \rangle \right] \\ &\stackrel{\text{Lemma 2.2}}{=} \left\langle \beta \left| \frac{df}{dy} \right|^2 \right\rangle + \left[\left\langle \beta \frac{df}{dy} \right\rangle \right] \langle \bar{f} \rangle \stackrel{\text{1st jump}}{=} \left\langle \beta \left| \frac{df}{dy} \right|^2 \right\rangle + \mathcal{K}[\mathbb{I}f] \langle \bar{f} \rangle \geq 0, \end{aligned}$$

hence the problem is non-negative. Therefore, in conclusion, the operator \mathcal{L} , together with the jump and periodicity conditions, is self-adjoint and non-negative.

Appendix B. Bloch-Floquet analysis of the monolayer case

In this case, u_δ satisfies (8) with $\alpha \equiv \beta \equiv 1$, hence, on $(0, \delta)$, we have

$$u_\delta(x) = A_{\text{BF}} \cos\left(\frac{\mu x}{\delta}\right) + B_{\text{BF}} \sin\left(\frac{\mu x}{\delta}\right), \quad (\text{B.1})$$

$$u'_\delta(x) = -\frac{A_{\text{BF}}\mu}{\delta} \sin\left(\frac{\mu x}{\delta}\right) + \frac{B_{\text{BF}}\mu}{\delta} \cos\left(\frac{\mu x}{\delta}\right), \quad (\text{B.2})$$

subject to the two jump conditions $\llbracket u_\delta \rrbracket_0 = \frac{\delta}{\mathcal{K}} \langle u'_\delta \rangle_0$ and $\delta \llbracket u'_\delta \rrbracket_0 = -m\mu^2 \langle u_\delta \rangle_0$, relating the value of u_δ and u'_δ at 0^+ and 0^- . Moreover, according to Bloch-Floquet theory, we know that

we can write $u_\delta(x) = u_\delta(x)e^{ikx}$, for a δ -periodic function u_δ , implying that, in particular, we have $u_\delta(\delta^-) = u_\delta(0^-)e^{ik\delta}$ and $u'_\delta(\delta^-) = u'_\delta(0^-)e^{ik\delta}$. This, combined with the jump conditions, relates the values of u_δ and u'_δ at 0^+ and δ^- , and hence it gives two equations on A_{BF} and B_{BF} . These equations can be summarised by a matrix equation of the form $\mathcal{M}_{\text{BF}}^{\text{mo}}(\mu, \kappa\delta, m, \ell)(A_{\text{BF}}, B_{\text{BF}})^T = (0, 0)^T$, where

$$\mathcal{M}_{\text{BF}}^{\text{mo}} = \begin{pmatrix} 1 - e^{-ik\delta} \cos(\mu) + \frac{\mu}{2\ell} \sin(\mu)e^{-ik\delta} & -\sin(\mu)e^{-ik\delta} - \frac{\mu}{2\ell}(1 + \cos(\mu)e^{-ik\delta}) \\ -\mu \sin(\mu)e^{-ik\delta} - \frac{m\mu^2}{2}(1 + \cos(\mu)e^{-ik\delta}) & -\mu(1 - \cos(\mu)e^{-ik\delta}) - \frac{m\mu^2}{2} \sin(\mu)e^{-ik\delta} \end{pmatrix}.$$

One notes that, as expected, for $\kappa\delta = 0$ or $\kappa\delta = \pi$ we have $\mathcal{M}_{\text{BF}}^{\text{mo}} = \mathcal{M}^{\text{mo}}$ with the relevant sign. Of course, this system has only non-trivial solutions if $\det(\mathcal{M}_{\text{BF}}^{\text{mo}}) = 0$. A little bit of algebra shows that

$$\det(\mathcal{M}_{\text{BF}}^{\text{mo}}) = \mu \left(-\mathcal{B} + 2e^{-ik\delta} \left(C \cos(\mu) - \frac{1}{2} \left(\frac{1}{\ell} + m \right) \mu \sin(\mu) \right) - \mathcal{B}e^{-2ik\delta} \right),$$

where $\mathcal{B} = 1 + \frac{m\mu^2}{4\ell}$ and $C = 1 - \frac{m\mu^2}{4\ell}$. Equating it to zero and multiplying by $e^{ik\delta}/(\mathcal{B}\mu)$, this leads to the dispersion relation (75). For a value of μ satisfying the dispersion relation, we have infinitely many possible $(A_{\text{BF}}, B_{\text{BF}})^T$. To find one, just fix $A_{\text{BF}} = 1$, and use either the first or second line of $\mathcal{M}_{\text{BF}}^{\text{mo}}$ to get B_{BF} as follows:

$$B_{\text{BF}} = \frac{1 + e^{-ik\delta} \left(-\cos(\mu) + \frac{\mu}{2\ell} \sin(\mu) \right)}{\frac{\mu}{2\ell} + e^{-ik\delta} \left(\sin(\mu) + \frac{\mu}{2\ell} \cos(\mu) \right)} \quad \text{or} \quad B_{\text{BF}} = \frac{\frac{m\mu}{2} + e^{-ik\delta} \left(\sin(\mu) + \frac{m\mu}{2} \cos(\mu) \right)}{-1 + e^{-ik\delta} \left(\cos(\mu) - \frac{m\mu}{2} \sin(\mu) \right)},$$

depending on which one has a non-zero denominator. It then leads to the exact Bloch-Floquet solution $u_\delta(x)$ on $(0, \delta)$. From this we recover $u_\delta(x) = u_\delta(x)e^{-ikx}$ on $(0, \delta)$, which we can extend to $x \in \mathbb{R}$ by periodicity. We can therefore get $u_\delta(x)$ everywhere by $u_\delta(x) = u_\delta(x)e^{ikx}$.

- [1] A. Bensoussan, J.-L. Lions, G. Papanicolaou, *Asymptotic analysis for periodic structures*, North-Holland, 1978.
- [2] N. Bakhvalov, G. Panasenko, *Homogenisation: averaging process in periodic media*, Kluwer Academic Publishers, 1984.
- [3] D. Cioranescu, P. Donato, *An Introduction to Homogenization*. Oxford lecture series in mathematics and its applications, Vol. 17, OUP, 1999. doi:10.14708/ma.v28i42/01.1882.
- [4] V. Laude, *Phononic Crystals: Artificial Crystals for Sonic, Acoustic, and Elastic Waves*, De Gruyter, 2015.
- [5] T. Gorishnyy, M. Maldovan, C. Ullal, E. Thomas, *Sound ideas*, *Physics World* 18 (12) (2005) 24–29. doi:10.1088/2058-7058/18/12/30. URL <https://doi.org/10.1088/2058-7058/18/12/30>
- [6] R. V. Craster, J. Kaplunov, A. V. Pichugin, *High-frequency homogenization for periodic media*, *Proc. R. Soc. A* 466 (2120) (2010) 2341–2362. doi:10.1098/rspa.2009.0612.
- [7] B. B. Guzina, S. Meng, O. Oudghiri-Idrissi, *A rational framework for dynamic homogenization at finite wavelengths and frequencies*, *Proc. R. Soc. A* 475 (2223) (2019) 1–29. arXiv:1805.07496, doi:10.1098/rspa.2018.0547.
- [8] S. Meng, O. Oudghiri-Idrissi, B. B. Guzina, *A convergent low-wavenumber, high-frequency homogenization of the wave equation in periodic media with a source term*, arXiv preprint 2002.028338v1 (2020) 1–25 arXiv:2002.02838. URL <http://arxiv.org/abs/2002.02838>
- [9] D. Harutyunyan, G. W. Milton, R. V. Craster, *High-frequency homogenization for travelling waves in periodic media*, *Proc. R. Soc. A* 472 (2191) (2016) 20160066. doi:10.1098/rspa.2016.0066. URL <https://doi.org/10.1098/rspa.2016.0066>
- [10] E. Nolde, R. Craster, J. Kaplunov, *High frequency homogenization for structural mechanics*, *J. Mech. Phys. Solids* 59 (3) (2011) 651–671. doi:10.1016/j.jmps.2010.12.004. URL <https://doi.org/10.1016/j.jmps.2010.12.004>

- [11] D. J. Colquitt, R. V. Craster, M. Makwana, [High frequency homogenisation for elastic lattices](#), *Q. J. Mech. Appl. Math.* 68 (2) (2015) 203–230. doi:10.1093/qjmam/hbv005.
URL <https://doi.org/10.1093/qjmam/hbv005>
- [12] I. Sevostianov, R. Rodríguez-Ramos, R. Guinovart-Díaz, J. Bravo-Castillero, F. J. Sabina, [Connections between different models describing imperfect interfaces in periodic fiber-reinforced composites](#), *J. Mech. Solid. Struct.* 49 (13) (2012) 1518–1525. doi:10.1016/j.ijjstr.2012.02.028.
URL <http://dx.doi.org/10.1016/j.ijjstr.2012.02.028>
- [13] Y. C. Angel, J. D. Achenbach, Reflection of ultrasonic waves by an array of microcracks, in: D. Thompson, D. Chimenti (Eds.), *Review of Progress in Quantitative Nondestructive Evaluation*, Springer, 1985, pp. 83–89.
- [14] A. Pilarski, J. L. Rose, [A transverse-wave ultrasonic oblique-incidence technique for interfacial weakness detection in adhesive bonds](#), *Journal of Applied Physics* 63 (2) (1988) 300–307. doi:10.1063/1.340294.
URL <https://doi.org/10.1063/1.340294>
- [15] A. Pilarski, J. L. Rose, K. Balasubramaniam, [The angular and frequency characteristics of reflectivity from a solid layer embedded between two solids with imperfect boundary conditions](#), *J. Acoust. Soc. Am.* 87 (2) (1990) 532–542. doi:10.1121/1.398924.
URL <https://doi.org/10.1121/1.398924>
- [16] M. Schoenberg, [Elastic wave behavior across linear slip interfaces](#), *J. Acoust. Soc. Am.* 68 (5) (1980) 1516–1521. doi:10.1121/1.385077.
URL <https://doi.org/10.1121/1.385077>
- [17] J.-M. Baik, R. B. Thompson, [Ultrasonic scattering from imperfect interfaces: A quasi-static model](#), *J. Nondestruct. Eval.* 4 (3-4) (1984) 177–196. doi:10.1007/bf00566223.
URL <https://doi.org/10.1007/bf00566223>
- [18] S. I. Rokhlin, Y. J. Wang, [Analysis of boundary conditions for elastic wave interaction with an interface between two solids](#), *J. Acoust. Soc. Am.* 89 (2) (1991) 503–515. doi:10.1121/1.400374.
URL <https://doi.org/10.1121/1.400374>
- [19] P. P. Delsanto, M. Scalerandi, [A spring model for the simulation of the propagation of ultrasonic pulses through imperfect contact interfaces](#), *J. Acoust. Soc. Am.* 104 (5) (1998) 2584–2591. doi:10.1121/1.423841.
URL <https://doi.org/10.1121/1.423841>
- [20] H. G. Tattersall, [The ultrasonic pulse-echo technique as applied to adhesion testing](#), *J. Phys. D* 6 (7) (1973) 819–832. doi:10.1088/0022-3727/6/7/305.
URL <https://doi.org/10.1088/0022-3727/6/7/305>
- [21] C. Licht, F. Lebon, A. Léger, Dynamics of elastic bodies connected by a thin adhesive layer, in: A. Leger, M. Deschamps (Eds.), *Ultrasonic Wave Propagation in Non Homogeneous Media*, Vol. 128, Springer Proceedings in Physics, 2009, pp. 99–110.
- [22] C. Bellis, M. Touboul, B. Lombard, R. C. Assier, Effective dynamics for low-amplitude transient elastic waves in a 1d periodic array of non-linear interfaces, Submitted, preprint [Hal:02957419](https://hal.archives-ouvertes.fr/hal-02957419).
- [23] Z. Hashin, Thermoelastic properties of fiber composites with imperfect interface, *Mechanics of Materials* 8 (1990) 333–348.
- [24] Z. Hashin, Thin interphase/imperfect interface in elasticity with application to coated fiber composites, *J. Mech. Phys. Solids* 50 (12) (2002) 2509–2537. doi:10.1016/S0022-5096(02)00050-9.
- [25] J. C. López-Realpozo, R. Rodríguez-Ramos, R. Guinovart-Díaz, J. Bravo-Castillero, L. P. Fernández, F. J. Sabina, G. A. Maugin, Effective properties of non-linear elastic laminated composites with perfect and imperfect contact conditions, *Mech. Adv. Mater. Struc.* 15 (5) (2008) 375–385. doi:10.1080/15376490801977742.
- [26] J. P. Lee-Thorp, M. I. Weinstein, Y. Zhu, [Elliptic operators with honeycomb symmetry: Dirac points, edge states and applications to photonic graphene](#), *Arch. Ration. Mech. Anal.* 232 (1) (2018) 1–63. doi:10.1007/s00205-018-1315-4.
URL <https://doi.org/10.1007/s00205-018-1315-4>
- [27] T. Ochiai, M. Onoda, [Photonic analog of graphene model and its extension: Dirac cone, symmetry, and edge states](#), *Phys. Rev. B* 80 (15). doi:10.1103/physrevb.80.155103.
URL <https://doi.org/10.1103/physrevb.80.155103>
- [28] R. Moukhomdiarov, A. Pichugin, G. Rogerson, [The transition between neumann and dirichlet boundary conditions in isotropic elastic plates](#), *Math. Mech. Solids* 15 (4) (2010) 462–490. [arXiv:https://doi.org/10.1177/1081286509103781](https://arxiv.org/abs/https://doi.org/10.1177/1081286509103781), doi:10.1177/1081286509103781.
URL <https://doi.org/10.1177/1081286509103781>
- [29] R. Penrose, [A generalized inverse for matrices](#), *Math. Proc. Cambridge* 51 (3) (1955) 406–413. doi:10.1017/s0305004100030401.
URL <https://doi.org/10.1017/s0305004100030401>